

Unterschrift des Betreuers



TECHNISCHE
UNIVERSITÄT
WIEN
Vienna University of Technology

DIPLOMARBEIT

Modelling and Simulation of Competitive Crystal Growth

Theory, Implementation and Simulation of the Van der Drift Model

Ausgeführt am

Institut für Mikroelektronik
der Technischen Universität Wien

unter der Anleitung von
Ao.Univ.Prof. Dipl.-Ing. Dr.techn. Erasmus Langer

Betreut von
Dipl.-Ing. Dr.techn. Hajdin Ceric
und
Dipl.-Ing. Dipl.-Ing. Karl Rupp

durch

Valentin Schnitzer

Baumannstr. 5/15
1030 Wien

Matrikelnummer 0225549
Studienkennzahl 869

Datum

Unterschrift

Abstract

Residual stresses determine the mechanical properties of metal films. To model these, numerous models based on continuum mechanics have been created which are applicable only for simplified situations. To investigate more sophisticated situations, crystal microstructure morphology simulations can be used as basis. However for this approach the results need to be in a format usable for the subsequent stress simulations. This is possible for the algorithm described in the course of this work, which is based on the Van der Drift model. The approach taken in the creation of the algorithm is flexible and allows for more general cases than previous algorithmic formulations of the model. The program implemented on basis of this algorithm is capable of exporting a mesh usable for the simulation of stress by the finite element method. In addition to the algorithm and its implementations the scaling of the average in-plane crystal size and the a possible extension of the model are investigated. These theoretical results are then used for the simulations and for the analyse of their results.

Contents

1	Crystal Growth	7
1.1	Overview	7
1.2	Simulation Models	7
2	Scaling of the Average In-Plane Crystal Size	9
2.1	Introduction	9
2.2	Square Crystals	11
2.3	Right-Angled Triangles	18
3	An Algorithm for the Van der Drift Model	22
3.1	Possible Events on a Crystal Side	24
3.2	Identification of Events	30
3.3	Technical Implementation	32
4	An Extension of the Van der Drift Model	35
4.1	Surface Diffusion Restricted to a Crystal	35
4.2	Surface Diffusion Partially Restricted to Crystals	39
5	Simulation	41
5.1	Infinite Surface Diffusion on the Film	41
5.2	Infinite Surface Diffusion Restricted to a Crystal	46
5.3	General Two-dimensional Cases	55
6	Conclusion and Outlook	57

List of Figures

1.1	Volmer-Weber Growth	8
2.1	Characterization of the Orientation of a Square Crystal	11
2.2	Two Crystals Overlap	13
2.3	Magnification of the Overlap	13
2.4	Growth of a Triangular Crystal	19
2.5	Embedding a Square in a Triangle Crystal	21
3.1	Example for the Van der Drift Growth Model	23
3.2	The Two Growth Rules Used by Van der Drift	24
3.3	Vertex Hits Side	25
3.4	Fusion of Three Sides	26
3.5	First Type of Overgrowth	27
3.6	Second Type of Overgrowth	28
3.7	Model Problem	29
3.8	Small Side After Side Splitting	30
3.9	Missed Deletion	31
3.10	Overgrowth Problem	32
3.11	Program Flow	33
3.12	Program Structure	34
4.1	Needle	36
4.2	Surface of a Right-Angled Triangle	36
4.3	Model Problem	38
5.1	Simulation Results Starting with Squares	42
5.2	Simulation Results Starting with Right-Angled Triangles	42
5.3	Number of Square Crystals over Time	43
5.4	Number of Square Crystals over Time (Logarithmic Scales)	43
5.5	Number of Right-Angled Triangular Crystals over Time	44
5.6	Number of Right-Angled Triangular Crystals over Time (Logarithmic Scales)	44
5.7	Remaining Angles Starting with a Uniform Distribution	45
5.8	Number of Crystals over Time ($\theta = 0.7 \pi$)	46
5.9	Number of Crystals over Time ($\theta = 0.7 \pi$, Logarithmic Scales)	47
5.10	Number of Crystals over Time ($\theta = 0.3 \pi$)	47
5.11	Number of Crystals over Time ($\theta = 0.3 \pi$, Logarithmic Scales)	48

5.12	Number of Crystals over Time ($\theta = 0.5 \pi$)	48
5.13	Number of Crystals over Time ($\theta = 0.5 \pi$, Logarithmic Scales)	49
5.14	Material from the Middle, Material Diffusion Restricted to the Crystals . .	50
5.15	Material from the Middle, 75% Material Diffusion Restricted to the Crystals	50
5.16	Material from the Middle, 50% Material Diffusion Restricted to the Crystals	51
5.17	Material from the Left	51
5.18	Material from the Right	52
5.19	Material from the Right, Material Diffusion Restricted to the Crystals . . .	52
5.20	Material from the Right, 75% Material Diffusion Restricted to the Crystals	53
5.21	Material from the Right, 50% Material Diffusion Restricted to the Crystals	53
5.22	Number of Crystals over Time, Material Coming from The Right	54
5.23	Simulation Result for Material from the right and 50% Material Diffusion restricted to the Crystals	54
5.24	Crystals Growing in a Valve	55
5.25	A General Two-dimensional Case	56

Acknowledgement

I like to thank all people, which in one way or another assisted me in my work.

Introduction

The manufacturing process of metal layers produces large residual stresses which are built during the process itself or thereafter. These residual stresses determine the mechanical properties of metal films. In the case of interconnect reliability, the residual stresses play a significant role for electromigration failure. Such residual stresses arise from two main sources. First, there is the tendency of copper to shrink or expand, once deposited on the substrate, and second there is the thermal mismatch between adjacent layers. Generally, thin films change their volume during the deposition process itself and aftermath due to the evolution of the metal microstructure [9, 16] thus generating microstrains.

The lack of appropriate measurements makes it impossible to obtain detailed stress load distributions as necessary for an assessment of metallization reliability. The realistic material properties of an interconnect tightly packed in surrounding layers depend on its geometry and grain size effects and are also hardly reachable by experimental means [7].

The distribution of the stress which arises due to microstrains strongly depends on the morphology of the grains. Different aspects of the connection between microstructure and stress have been investigated in the last 30 years. The focus was mainly on some specific grain-grain boundary configurations in early or mature stages of microstructure evolution [16]. As a result, numerous models on the basis of continuum mechanics have been derived, which are applicable only for highly simplified situations. For example, the model of Nix [27] describes the initial build-up of tensile stress during Volmer-Weber crystal growth with a simple hexagonal grain morphology. In turn, Sheldon et al. [2] describes the rise of compressive stress in a late phase of film growth. Again, grains with simple geometries are assumed, with grain boundaries perpendicular to the substrate surface. In deriving the model it has been assumed that the stress in the film is determined by mechanisms that operate at the grain boundaries and that it is a result of insertion of excess adatoms at grain boundaries. Parallel to the development of mechanical models, a group of researchers, mostly mathematicians, have developed complex models for describing the morphology of the microstructural evolution. The study was initiated by the work of Van der Drift [1], which has introduced an algorithm for competitive grain growth capable of reproducing the network of grain boundaries. The work on microstructure morphology culminates in multi-level-set models of grain evolution [20, 22]. Even though these models do not include any stress generation mechanisms, they can reproduce microstructures with a high degree of accuracy and provide a basis for the investigation of grains size statistics [3], which can then be used as an input for stress calculations [8]. By this means the stress distribution of a copper film on a TaN/SiO₂ layer [9] and of a fixed or deflected cantilever [10] have been simulated.

To directly use results of morphology simulations without using statistical parameters for the transfer, typically a mesh is needed for the discretisation of the underlying system of

equations. On this mesh the stress simulations can be carried out for example using the finite element method. The generation of such a mesh is difficult to do in the case of the level-set method but easily done in case of the Van der Drift model. An algorithm for this model is given and a program is implemented which is capable of generating a mesh needed for stress simulations.

Before looking at the Van der Drift model, all phases of crystal growth are enumerated and an overview over the different possible simulation models is given. It is succeeded by the investigation of the scaling of the average in-plane crystal size and the asymptotical behaviour based on the proof by Thijssen, Knops and Dammers [15]. The proof is extend to a starting configuration consisting of right-angled triangles instead of squares. After this, the layout of the algorithm is given and the restrictions needed for the simulation of a case where the diffusion is limited to a crystal are discussed. Finally, the simulation results are compared with the theoretical results and examples are given of other possibilities for simulations that stem from the approach taken in the construction of the algorithm.

Chapter 1

Crystal Growth

1.1 Overview

There are different possibilities for creating thin crystal films: electrodeposition, growth from liquid solutions or from melts and the most common, growth through condensation from vapour. The process and its parameters influence the microstructural development which determines the residual stresses present in a film.

One type of growth from vapour is the Volmer-Weber growth (see figure 1.1). In the early stage of growth of a metal film on a substrate by the Volmer-Weber mechanism, a tensile stress in the film is observed to arise, when islands of deposited material begin to coalesce. The mechanism commonly proposed as the origin of this tensile stress is that the coalescing islands deform in order to form a relatively low energy grain boundary, at the expense of surface energy due to the surface area reduction. This mechanism proceeds until a stress magnitude sufficient to prevent further area reduction is generated. This initial phase is followed by competitive grain growth and an insertion of atoms from the film surface into the grain boundaries. Therefore, the Volmer-Weber mechanism represents a complex process of interaction between microstructure evolution and stress build-up.

In the following chapters the Van der Drift model is used to approximate the morphology of Volmer-Weber growth, or more exactly, Type 1 thickening as shown in figure 1.1. There are different models and a short overview of them is given.

1.2 Simulation Models

The first type of models in this overview is based on the Monte Carlo method and simulate the dynamics of atoms or small particles. Since the crystals are composed out of numerous small objects, which can be handled individually, many details of the simulation can be controlled. However, as large amounts of data have to be handled, most simulations are two dimensional or limited to a few atomic layers. Examples can be found in [12, 19] or more recently [23].

Alternatively the crystals of the film can be modelled by a set of functions. There are two different governing equations which can be used for this: The phase model [13, 14, 18, 24] and the level set method [6, 20]. Using these formulations, the solution is approximated by the use of an appropriate discretization.

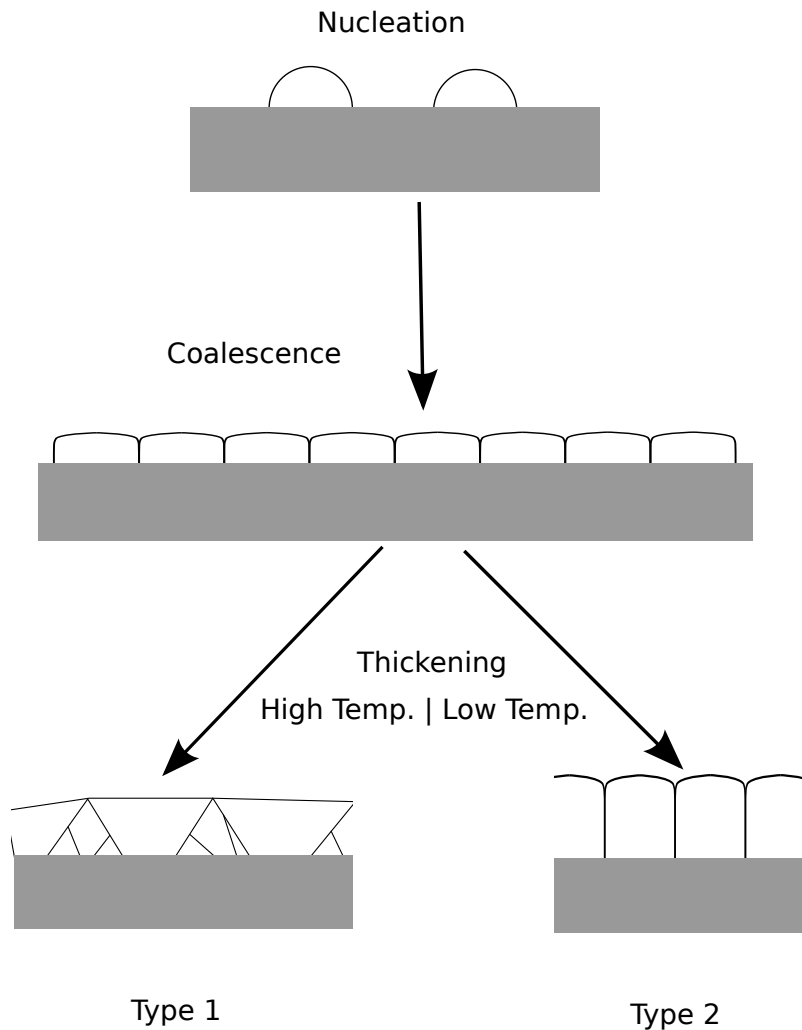


Figure 1.1: Volmer-Weber Growth

To get a grid for stress simulations using the e.g. finite element method, an interpolation of the grain boundaries is needed. Instead of using these approaches, which require post-processing to fit the requirements for the algorithm given in this work, the Van der Drift model [1] is used. Since it uses the grain boundaries as the main means to simulate the growth, the generation of the grid is straightforward. The details of this model are discussed in the next chapters.

Chapter 2

Scaling of the Average In-Plane Crystal Size

In this chapter we look at the scaling of the average in-plane crystal size which is part of the important structural characteristics of a crystal film, among crystal shapes, crystal sizes, the distribution of crystal sizes and the distribution of the crystal orientations in a crystal film. By in-plane size of a crystal we define the area the crystal occupies in an intersecting plane which has the same orientation as the plane the material is deposited on, which we call substrate. If the area of the crystals increases, in turn the number of crystals decreases given the space limitation on the substrate. For this reason we can deduct how coarse the surface of the crystal film is. In particular we look at the 2D Van der Drift model, for which also a description of a numerical simulation follows in the next chapter.

2.1 Introduction

The 2D Van der Drift model is a model for competitive crystal growth at the surface of growing films after a continuous film has formed. An overview of all phases is given in [4]. This competitive growth is often described as evolutionary selection, as only crystals with the most favourable characteristics remain at the surface or - to put it in the terms of an evolutionary process - survive. In such a model the reduction of the number of crystals is a result of evolutionary selection. Therefore, it can be quantified how far the selection has evolved and how uniformly, in the sense of the characteristics of its crystals, the film is structured on the surface.

Definition 1 (Growth of the average in-plane crystal size). *Let $\xi(t)$ be the average in-plane crystal size at t . We define the growth rate p by the following asymptotic relation for large t :*

$$\xi(t) \sim t^p \Leftrightarrow p \sim \frac{\ln(\xi(t))}{\ln t}. \quad (2.1)$$

The fact that the scaling of the average in-plane crystal size is polynomial has first been stated by Lifshitz and Slyozov [11] and found in the growth of silicon carbide films under various conditions by Roy and Messier [22].

Numerous models for this type of growth have been proposed with differing growth rates.

For example, the growth rate starting with a uniform distribution in the Huygens model is $1/3$ [3] in contrast to the lower bound of the growth rate of $1/2$ we prove for the 2D Van der Drift model. In this example the difference can be explained by the fact that the 2D Van der Drift model is a local model in contrast to the Huygens model, which is global. The difference between a local and a global model lies in its growth rules which describes it. The growth rules of a crystal in a local model is dependent on the crystals surrounding it, whereas in contrast the growth rules in a global model are independent of the local situation of a crystal.

We now take a closer look at the 2D Van der Drift model, for which we prove a lower bound of the growth rate. The model was first introduced in [1]. It describes crystal film growth, where the evolutionary selection happens out of the differences in height growth of the crystals. Therefore, in the long term the crystals which remain involved in the growth process on the surface are the ones which are orientated within a small derivation of the orientation with maximum growth. Van der Drift analyses these maxima for a variety of cases. For the case of infinite surface diffusion along the surface of the film for 2-dimensional crystals, he gives a graphical growth model, which we in short refer to as 2D Van der Drift model. This has been used model for example to explain crystal size and crystal film structure in diamond films [5].

In the 2D Van der Drift model the starting point is a set of convex polygons, describing the crystals of the film, of which either only a vertex or a whole side lies on the substrate. Because of the assumed infinite surface diffusion, the amount of material deposited per area on each of the side of the crystals is the same. This results in an equal growth speed in normal direction for all sides of all crystals of the film except those which describe boundaries between crystals or a crystal and the substrate as these are immobile. If during growth two crystals connect, a new boundary is formed, which is the result of the averaging of the growth of these sides. We explain this rule in more detail in the next chapter, where we also give an algorithm for the simulation of this model. As the sides grow, the area and the height of the crystals increase. The latter is defined as the maximum distance of a vertex of crystal to the substrate. Even though the height of the crystal can be defined by differing vertices during growth, the most important vertex for survival in the long term is the vertex which describes it at the start. If this vertex, which we also call the top vertex, is not defining the height any longer, it has been covered by a side of another crystal with greater height. The top also has the fastest height growth, therefore the other vertices get overgrown in the end by either the crystal which covered the top or another. Hence there is no chance of survival in the long term once the top vertex has been covered.

In the following sections we prove a lower bound for the growth of the average in-plane crystal size using two different starting configurations of the crystal film. We use the proof from Thijssen, Knops and Dammers [15] as a starting point for the proof for the first configuration. They state that their proof suffices to show asymptotical equivalence, which it does not. The reasons for this and other differences are given at the end of the following section.

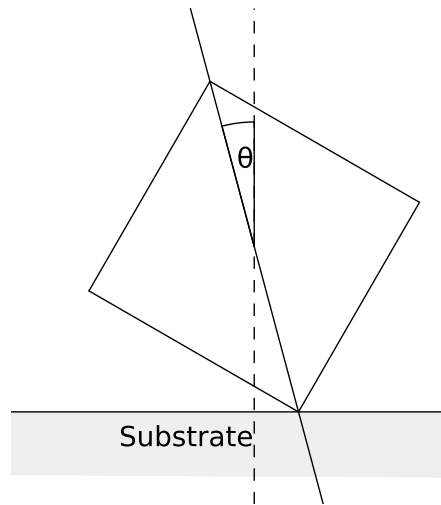


Figure 2.1: Characterization of the Orientation of a Square Crystal

2.2 Square Crystals

In this section we look at films consisting of square crystals of equal size and differing orientations. Because of the reasons already given, the most important quantity regarding survival is the top vertex. Therefore, we define the orientation of the square crystals using the top vertices of the crystals.

Definition 2 (Orientation of a square crystal). *Given a square crystal in the starting configuration. Then the orientation of the crystal is given by the angle between the diagonal from the top vertex to the vertex on the substrate and the normal vector of the substrate.*

From this definition follows that the possible values for θ are in the range of $(-\frac{\pi}{4}, \frac{\pi}{4})$. To calculate the average in-plane crystal size directly, we need to know the geometry of every crystal in the film. This geometric information is normally gathered by simulation, because it is nearly impossible by theoretical means in all but the simplest cases. Therefore, we look at the number of crystals, which survived until certain time, and divide the length of the substrate by it. This amounts to the same values as the sum of all in-plane crystal sizes equals the length of the substrate. For this reason we look at the number of crystals and use the reciprocal relation to analyse the long term behaviour.

Definition 3. *We define*

$$N(\theta, t)$$

as the number of square crystals with orientation θ which survived until time t . Here, survival means that the top vertex of the crystal has not been covered by any other crystal.

The type of survival used in this definition has one shortcoming: The average in-plane crystal size calculated from it is not always equal to measurements on the surface of the film. The reason is that a side of a crystal can remain at the surface of the crystal film even though the top of the crystal has been covered. This results in a measured average in-plane crystal size which is lower than the value calculated using the number of surviving

crystals. But this is only a momentary situation.

As $N(\theta, t)$ denotes the number of squares with angle θ to survive until time t , $N(\theta, 0)$ is therefore the initial distribution of the number of square crystals in dependence of its angle. Integration over all possible θ yields the number of surviving crystals at time t , which are used to calculate the average in-plane crystal size.

Definition 4 (Survival Probability). *Let $N(\theta, t)$ be the number of squares with angle θ to survive until time t . Then the survival probability for a seed with angle θ is given by:*

$$S(\theta, t) = \frac{N(\theta, t)}{N(\theta, 0)}. \quad (2.2)$$

Note that the survival probability also has a reciprocal connection to the growth rate as it is only normalized by the number of crystals at time $t = 0$. This means that a backward transformation only yields an additional constant with regard to the asymptotic behaviour. The reason for the introduction of this quantity is that we can handle the influences altering it, as we can give the exact circumstances when a crystal top is covered - or, in other terms the crystal, is overlapped.

Definition 5 (Base Point). *We define the Base Point of a vertex as the bottom vertex in the starting configuration.*

Lemma 1. *Given an overlap of two square crystals which base points are a distance x apart, with orientations $\theta \geq 0$ and $\theta' \geq 0$, respectively. The distance of the base point to the top vertex for both crystals is d . Furthermore, the right crystal overlaps the left (see figure 2.2). Under these conditions the following equation holds:*

$$\sin \theta + \sin \theta' + (\cos \theta' - \cos \theta) \tan \left(\frac{\pi}{4} - \theta' \right) = \frac{x}{d} \quad (2.3)$$

For the case of an overlap of the right crystal by the left we get:

$$\sin \theta + \sin \theta' + (\cos \theta - \cos \theta') \tan \left(\frac{\pi}{4} - \theta \right) = \frac{x}{d} \quad (2.4)$$

Proof. We start with the proof for $\theta \geq \theta'$. For this we compose x out of three parts which are all part of different right-angled triangles.

$$x = x' + x'' + x''' \quad (2.5)$$

For the first two parts x' and x''' we use the sine-theorem:

$$\frac{x'}{\sin \theta} = \frac{y}{\sin \left(\frac{\pi}{2} - \theta \right)} \Leftrightarrow x' = \frac{y \sin \theta}{\sin \left(\frac{\pi}{2} - \theta \right)} = \frac{y \sin \theta}{\cos \theta}, \quad (2.6)$$

$$\frac{x'''}{\sin \theta'} = \frac{y'}{\sin \left(\frac{\pi}{2} - \theta' \right)} \Leftrightarrow x''' = \frac{y' \sin \theta'}{\sin \left(\frac{\pi}{2} - \theta' \right)} = \frac{y' \sin \theta'}{\cos \theta'}. \quad (2.7)$$

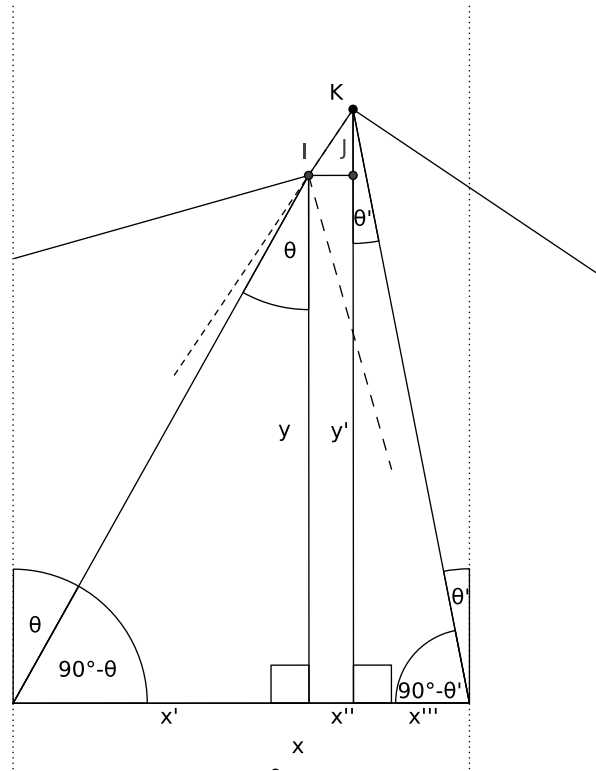


Figure 2.2: Two Crystals Overlap

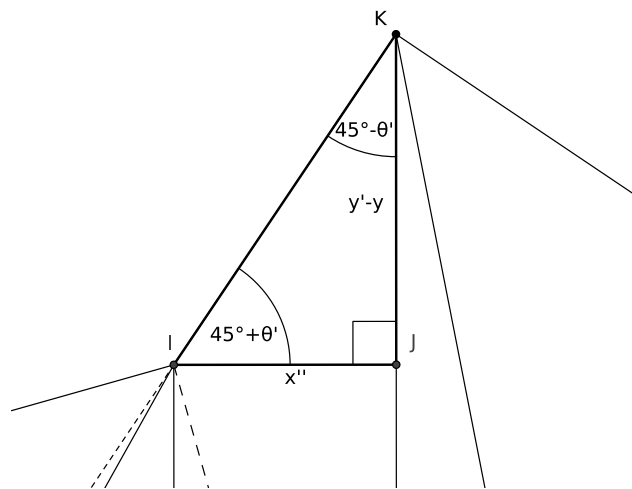


Figure 2.3: Magnification of the Overlap

Using the sine-theorem again on the triangle, which in contrast to the other properties stems from the intersection, we get:

$$\frac{x''}{\sin\left(\frac{\pi}{4} - \theta'\right)} = \frac{y' - y}{\sin\left(\frac{\pi}{2} - \left[\frac{\pi}{4} - \theta'\right]\right)} \quad (2.8)$$

$$\Leftrightarrow x'' = \frac{(y' - y) \sin\left(\frac{\pi}{4} - \theta'\right)}{\cos\left(\frac{\pi}{4} - \theta'\right)} = (y - y') \tan\left(\frac{\pi}{4} - \theta'\right) \quad (2.9)$$

To eliminate the occurrences of y we use the following properties of a right-angled triangle:

$$\frac{y}{d} = \cos \theta \quad \Leftrightarrow \quad y = d \cos \theta, \quad (2.10)$$

$$\frac{y'}{d} = \cos \theta' \quad \Leftrightarrow \quad y' = d \cos \theta'. \quad (2.11)$$

Now we put everything together:

$$x = \frac{y \sin \theta}{\cos \theta} + \frac{y' \sin \theta'}{\cos \theta'} + (y - y') \tan\left(\frac{\pi}{4} - \theta'\right), \quad (2.12)$$

$$\Leftrightarrow x = d \left(\frac{\cos \theta \sin \theta}{\cos \theta} + \frac{\cos \theta' \sin \theta'}{\cos \theta'} + (\cos \theta - \cos \theta') \tan\left(\frac{\pi}{4} - \theta'\right) \right), \quad (2.13)$$

$$\Leftrightarrow \frac{x}{d} = \sin \theta + \sin \theta' + (\cos \theta - \cos \theta') \tan\left(\frac{\pi}{4} - \theta'\right). \quad (2.14)$$

Looking at the case of $\theta \leq \theta'$ we note changes only in the small triangle at the top of (figure 2.3). The angles change dependence from θ' to θ and the height is $y - y'$ instead of $y' - y$. Therefore the equation transforms to:

$$\frac{x}{d} = \sin \theta + \sin \theta' + (\cos \theta' - \cos \theta) \tan\left(\frac{\pi}{4} - \theta\right). \quad (2.15)$$

□

Corollary 1. *Given an overlap of two square crystals whose bottom vertices are a distance x apart. The orientations of the crystals are θ and θ' , respectively. Let the size of both diagonals be d . If the crystal with orientation θ is overlapped, the following equation holds:*

$$\sin |\theta| + \sin |\theta'| + (\cos |\theta| - \cos |\theta'|) \tan\left(\frac{\pi}{4} - |\theta'|\right) = \frac{x}{d} \quad (2.16)$$

Proof. If $\theta \geq 0$ then $\theta \geq \theta' \geq 0$ which is the first case of lemma 1.

If $\theta \leq 0$ the overlapping crystal must lie to the left. Therefore, it is the second case of lemma 1 only swapping θ and θ' and taking the absolute value. □

Theorem 1. *Let $S(\theta, t)$ be the survival probability of a crystal with orientation θ and $P_d(\theta, t|\theta')$ the probability of a crystal with orientation θ to be overgrown at time t by a crystal with orientation θ' . Then*

$$\ln(S(\theta, t)) \leq -\frac{1}{\Delta_x} \int_0^{(\sqrt{2vt+d_0}) \sin |\theta|} \int_{\theta}^{\theta^*} P_d(\theta', t|\theta) d\theta' dx, \quad (2.17)$$

where $t'(\theta, \theta', x)$ is implicitly defined by

$$\sin |\theta| + \sin |\theta'| + (\cos |\theta| - \cos |\theta'|) \tan \left(\frac{\pi}{4} - |\theta'| \right) = \frac{x}{\sqrt{2}vt' + d_0} \quad (2.18)$$

with θ^* being the solution for θ' in this equation for the case $t' = t$, Δ_x being the distance between two adjacent squares, v the growth rate of a crystal edge in normal direction and d_0 the initial size of the diagonals of the crystals.

Proof. Suppose two squares which base points are x units apart (see figure 2.2), characterized by θ and θ' respectively. The growth rate of each side is v . Therefore, the lengths of the sides grow by $2vt$, hence the diagonal grows by $2\sqrt{2}vt$. The centre point of the crystals does not move, therefore, the growth in direction of the surface plays no part in the height growth the distance of the top vertex to the base point increases by $\sqrt{2}vt$.

We can express the survival probability for a time-step Δt by:

$$S(\theta, t) = \prod_{x, t'} (1 - P_d(x, t'|\theta)) \Delta t, \quad (2.19)$$

where $P_d(\theta, t|\theta')$ is the probability of a crystal with orientation θ to be overgrown at time t by a crystal with orientation θ' . To handle infinitesimal time-steps, we transform the product to a sum and in the end to an integral:

$$S(\theta, t) = \prod_{x, t'} (1 - P_d(x, t'|\theta)) \Delta t. \quad (2.20)$$

We use the inequality $\ln(1+x) \leq x$ for the right hand side of the equation to get the inequality:

$$\Leftrightarrow \ln S(\theta, t) = \sum_{x, t'} \ln((1 - P_d(x, t'|\theta)) \Delta t), \quad (2.21)$$

$$\Leftrightarrow \ln S(\theta, t) \leq - \sum_x \sum_{t'} P_d(x, t'|\theta) \Delta t, \quad (2.22)$$

$$\Leftrightarrow \ln S(\theta, t) \leq - \frac{1}{\Delta_x} \sum_x \sum_{t'} P_d(x, t'|\theta) \Delta_x \Delta t. \quad (2.23)$$

Note that in (2.23) we have two Riemann sums and therefore get a double integral for infinitesimal time-steps. Although the sum with respect to x seems to pose a problem at the first glance because of the fraction in front of the sum, it does not pose one as the distance of two crystals is constant and as a consequence the integral equals the sum.

We do not need to integrate over all possible values, only cases where $P_d(x, t'|\theta) \neq 0$. If this is the case, (2.18), which comes from corollary 1, holds and we can derive better limits for the integral:

$$\ln S(\theta, t) \leq - \frac{1}{\Delta_x} \int_0^t \int_0^{(\sqrt{2}vt+d_0) \sin |\theta|} P_d(x, t'|\theta) dx dt'. \quad (2.24)$$

The use of the complementary event to the survival of a crystal has the advantage that through x , t' and θ one distinct situation of interaction of two crystals is characterized, giving us the possibility to use (2.18) to transform the coordinates of our integrals.

$$\ln S(\theta, t) \leq \frac{1}{\Delta_x} \int_0^{(\sqrt{2vt+d_0}) \sin |\theta|} \int_{|\theta|}^{\theta^*} P_d(x, \theta'|\theta) d\theta' dx, \quad (2.25)$$

where θ^* is the solution of (2.18) for θ' for the case $t' = t$. □

Corollary 2. *Let $S(\theta, t)$ be the survival probability of a crystal with orientation $\theta \approx 0$. Then*

$$S(\theta, t) \leq e^{-\frac{3(\sqrt{2vt+d_0})\theta^2}{2\Delta_x}}. \quad (2.26)$$

Proof. To proof this we use theorem 1:

$$\sin |\theta| + \sin |\theta'| + (\cos |\theta| - \cos |\theta'|) \tan \left(\frac{\pi}{4} - |\theta'| \right) = \frac{x}{\sqrt{2vt+d_0}} \quad (2.27)$$

As we look at orientations near zero we can approximate $\sin \theta \approx \theta$ and $\cos \theta \approx 1$ and therefore both equation by:

$$|\theta'| \approx \frac{x}{\sqrt{2vt+d_0}} - |\theta| \quad (2.28)$$

We now use this approximation in conjunction with the upper bound of the probability $P_d(\theta', t|\theta) \leq 1$ to get:

$$\ln S(\theta, t) \leq \frac{1}{\Delta_x} \int_0^{(\sqrt{2vt+d_0}) \sin |\theta|} \int_{|\theta|}^{\theta^*} P_d(x, \theta'|\theta) d\theta' dx \quad (2.29)$$

$$\Rightarrow \ln S(\theta, t) \leq \frac{1}{\Delta_x} \int_0^{(\sqrt{2vt+d_0})|\theta|} \int_{|\theta|}^{\frac{x}{\sqrt{2vt+d_0}}} 1 d\theta' dx \quad (2.30)$$

$$\Rightarrow \ln S(\theta, t) \leq -\frac{3(\sqrt{2vt+d_0})}{2\Delta_x} \theta^2 \quad (2.31)$$

$$\Leftrightarrow S(\theta, t) \leq e^{-\frac{3(\sqrt{2vt+d_0})}{2\Delta_x} \theta^2} \quad (2.32)$$

□

Corollary 3. *Let $\xi(t)$ be the average size of a mono-crystalline domain at time $t \gg 0$, then:*

$$\xi(t) \geq \frac{\sqrt{v}}{\sqrt{\Delta_x}} t^{\frac{1}{2}} \tilde{c}(d_0), \quad (2.33)$$

where v is the growth rate of the sides of the square crystals in normal direction, Δ_x the distance between two crystals and d_0 the initial size of the diagonals. $\tilde{c}(d_0)$ is a constant dependent on d_0 .

Proof. For the previous corollary 2 to hold we need the orientations of the crystals to be near zero. We note that this is the case for $t \gg 0$ as the prevalent orientation for advanced stages of growth is near zero. This follows from the fact that a square with orientation θ can only be covered by another if the orientation of the other is smaller.

We therefore start with the previous corollary and integrate over all orientations to get the survival probability for all squares at time t and then use the inverse, which is up to a factor equal to the quantity we look for.

$$S(t) \leq \int_{-\frac{\pi}{4}}^{\frac{\pi}{4}} e^{-\frac{3(\sqrt{2}vt+d_0)}{2\Delta_x}\theta^2} d\theta \quad (2.34)$$

$$\leq 2 \int_0^{\infty} e^{-\frac{3(\sqrt{2}vt+d_0)}{2\Delta_x}\theta^2} d\theta = 2 \frac{\sqrt{\pi}}{2\sqrt{\frac{3(\sqrt{2}vt+d_0)}{2\Delta_x}}} = \frac{\sqrt{\sqrt{2}\pi}}{\sqrt{6}} \frac{\sqrt{\Delta_x}}{\sqrt{v}} t^{-\frac{1}{2}} \frac{1}{\sqrt{1 + \frac{d_0}{\sqrt{2}vt}}} \quad (2.35)$$

$$\leq \frac{\sqrt{\Delta_x}}{\sqrt{v}} t^{-\frac{1}{2}} c(d_0). \quad (2.36)$$

$c(d_0)$ is an upper bound for the factor dependent on d_0 , which is possible as the fraction in which it is involved tends to 1. Therefore:

$$\xi(t) \geq \frac{\sqrt{v}}{\sqrt{\Delta_x}} t^{\frac{1}{2}} \tilde{c}(d_0), \quad (2.37)$$

where $\tilde{c}(d_0)$ is the inverse of $c(d_0)$ and the factor needed to transform $S(t)$ to average in-plane size. \square

Now we want to highlight the problems in the paper [15].

- The deletion probability $P_d(x, t'|\theta)$ is dependent on θ , which the paper does not recognize or at least not emphasizes. This is problematic in so far that it is needed for the integral transformation to work.
- In the paper only one of the cases of overlap is looked at, namely a crystal getting overgrown from the right, and it does not state how it is connected to the other case.
- When

$$S(\theta, t) = \prod_{x, t'} (1 - P_d(x, t'|\theta)) \Delta_x \Delta_t \quad (2.38)$$

in the corresponding form is handled it is transformed to:

$$\ln S(\theta, t) = -\frac{1}{\Delta_x} \sum_x \sum_{t'} P_d(x, t'|\theta) \Delta_x \Delta_t. \quad (2.39)$$

This would imply $\ln(1-x) = -x$ which only has some validity in the case of $x \approx 0$. This is used without a word for its reason.

- They state:

$$P_d(x, t'|\theta) = \left| \frac{d\theta'(x, t', \theta)}{dt} \right| \tilde{P}(\theta', t'|\theta), \quad (2.40)$$

where $\tilde{P}(\theta', t'|\theta)$ is the probability of a square at distance x and orientation θ' in presence of a square with orientation θ to survive at time t' . This integral transformation has one problem: It is a coordinate transformation which transforms the deletion probability to the aforementioned survival probability. But these describe complementary events and because of this that it is not possible using a coordinate transformation as it does not change the value of the function.

- Next they use a mean-field type assumption:

$$\tilde{P}(\theta', t'|\theta) = P(\theta', t'). \quad (2.41)$$

This assumes - as they put it - that one can neglect the correlation of the orientations between the squares arising during growth. This assumption seems only being rectified in the paper by its similarity to the assumption in mean field theory [17]. The other problem with this equation is that $P(\theta', t')$ is the probability of a chosen square at time 0 to survive until time t' . This in turn means that one assumes even more than small correlation, which the paper mentions.

Because of these problems, we only followed the proof in the paper [15] up to the first problematic equation, which is more or less theorem 1.

For easier understanding, we introduced the survival probability using the number of crystals. In the paper, $P(\theta, t)$ is used, which is introduced as probability without an exact definition. It can be looked at as the ratio of surviving crystals with orientation θ at time t to the number of crystals present at time $t = 0$, which is a normalized form of the function used in this proof.

2.3 Right-Angled Triangles

Looking at the previous section, we note that only the upper part of the crystals are playing any part in the evolutionary process. Therefore, it would be of interest to have a look at a case without the bottom part, which had no influence in the survival. For this we can use right-angled triangles of which the bases lie on the substrate as a start. The question is if the growth fulfils the same inequality.

We start with a lemma, which gives us a connection of the starting angles of a triangle to its height growth rate (see figure 2.4).

Lemma 2. *Let v be the growth of the side b in normal direction in one time-step. Then the height of the triangle increases by*

$$h' = \frac{\sin(\beta)}{\sin(\alpha + \beta)} v \Delta t. \quad (2.42)$$

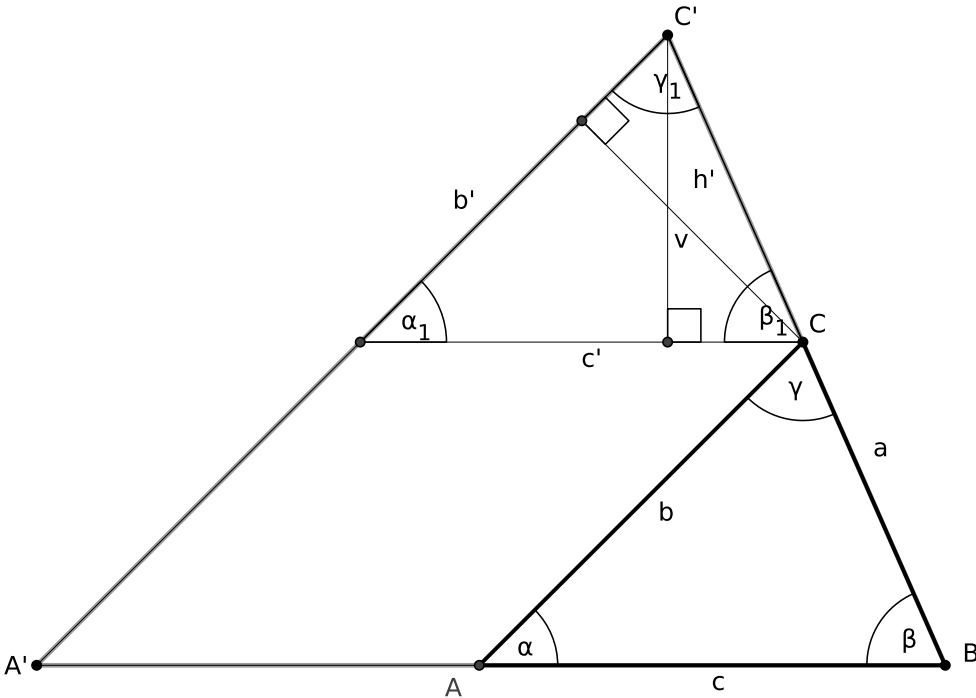


Figure 2.4: Growth of a Triangular Crystal

Proof. The first thing we notice is that $\alpha = \alpha_1$, $\beta = \beta_1$ and $\gamma = \gamma_1$, because the triangles ABC and $A'BC'$ are similar. To get to an expression for the increase in height we need two properties of the small triangle at the top. The first is a relation using the area of the triangle:

$$\frac{h'c'}{2} = \frac{b'v}{2} \quad \Leftrightarrow \quad h' = \frac{b'v}{c'}. \quad (2.43)$$

The second uses the law of sine:

$$\frac{c'}{\sin(180 - \alpha - \beta)} = \frac{b'}{\sin(\beta)} \quad \Leftrightarrow \quad b' = \frac{c' \sin(\beta)}{\sin(180 - \alpha - \beta)}. \quad (2.44)$$

Putting these two properties together, we get to:

$$h' = \frac{c' \sin(\beta)v}{c' \sin(180 - \alpha - \beta)} = \frac{\sin(\beta)}{\sin(\alpha + \beta)}v. \quad (2.45)$$

□

Corollary 4. *Let v_1 be the growth of the side b and v_2 be the growth of the side a . Then we get for the height increase h' the following equation:*

$$h' = \frac{\sin(\beta)}{\sin(\alpha + \beta)}v_1\Delta_t + \frac{\sin(\alpha)}{\sin(\alpha + \beta)}v_2\Delta_t \quad (2.46)$$

Proof. Using Lemma 2 and symmetry we obtain the property. □

Theorem 2. *Let $\xi(t)$ be the average in-plane crystal size at time $t \gg 0$, then:*

$$\xi(t) \geq \frac{\sqrt{v_t}}{\sqrt{\Delta_x}} t^{\frac{1}{2}} \tilde{c}(c_h), \quad (2.47)$$

where Δ_x is the minimum distance between two bottom vertices of the inlaid squares in the film, v_t the speed in normal direction at which the sides of the triangle grow, and c_h is the constant in the equation $h_0 = c_h (\sin \alpha + \sin \beta)$ for the initial height, where α and β are the angles of the sides to the base of the triangle.

Proof. The idea is to embed square crystals in the triangular crystals. Then we can use the proof of corollary 3 to prove the inequality.

Looking at figure 2.5, we get the following relation between the height h of the triangle and the diagonal d of the square:

$$d = \frac{h}{\sin\left(\frac{\pi}{4} + \alpha\right)}. \quad (2.48)$$

We now use the values of d and h for the particular case of this proof and then use corollary 3 in conjunction with corollary 4. The size d in our proof is different to the quantity used in the proof of 3, where only the part above the substrate is measured instead of the whole

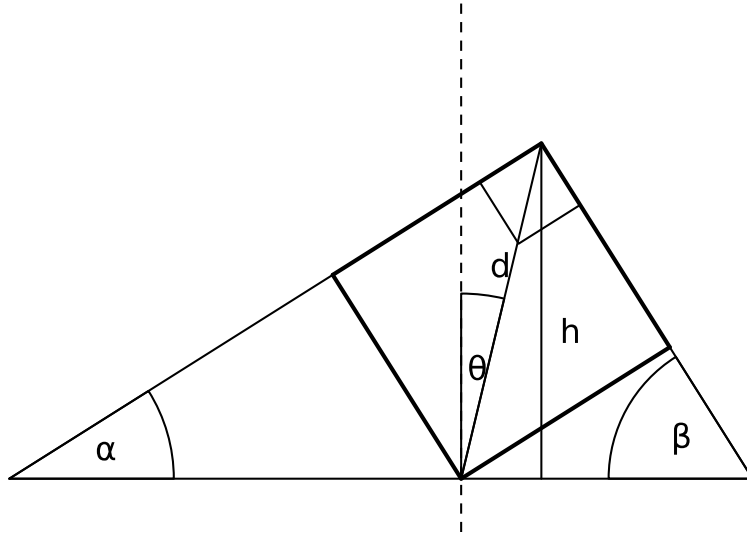


Figure 2.5: Embedding a Square in a Triangle Crystal

diagonal. As the square grows, the diagonal grows at twice the speed of the length from the bottom to the top vertex. Taking this into account, we get:

$$2\sqrt{2}vgt + d_0 = \frac{h_0 + (\sin \beta + \sin \alpha) v_t t}{\frac{1}{\sqrt{2}} (\sin \alpha + \sin \beta)}, \quad (2.49)$$

$$\Leftrightarrow 2\sqrt{2}vgt + d_0 = \sqrt{2}v_t t + \frac{\sqrt{2}h_0}{(\sin \alpha + \sin \beta)}, \quad (2.50)$$

$$\Leftrightarrow 2\sqrt{2}vgt + d_0 = \sqrt{2}v_t t + \sqrt{2}c_h. \quad (2.51)$$

We see that we can view the configuration as a film consisting of square crystals. The survival of the two geometrical objects is equal because the top of a triangle is only covered if the top of its square is covered. For this reason, the survival probability for both is the same. We still have to cope with the varying distances of the bottom vertices of the inlaid squares, because we considered square crystals spaced equidistantly in the previous section. But the only influence the spacing had on the derivation was as a factor for the integral. Therefore, to circumvent this problem we can use the minimum distance of two squares as this gives us an upper bound for $\frac{1}{\Delta_x}$. \square

To draw a connection to the previous section, we have varying starting heights for the different orientations of the triangles in this setting. But the initial height only has short term influence in the evolution as the differences in height growth will dominate in the long term. Therefore it still holds true in the long term for other starting configurations with the exclusion of extreme deviations.

Chapter 3

An Algorithm for the Van der Drift Model

With the algorithm presented in this chapter we take a new approach to the Van der Drift model. A rigorous comparison is difficult because most papers focus on the results of their algorithms rather than on the details of the algorithm.

Since its introduction in [1], the Van der Drift model has been implemented in a variety of ways based on the construction given by Van der Drift. Initially it was used for the case of square crystals growing on a line representing the substrate in the way shown in figure 3.1.

In addition to the result of an example crystal configuration, the two construction rules used for the configuration are given (see figure 3.2). To apply these rules, information about the neighbours of all crystals are needed. A neighbour of a crystal is a crystal which has or will have an inter-crystalline boundary with it. Such an approach was taken by A. J. Dammers and S. Radelaar in [26], where they used the so-called "winged edge" data structure to hold this information. An extension of this algorithm to a more general setting is complicated, because neighbour information is needed for the interaction of two crystals. This is due to the two construction rules, which use the boundaries of the two interacting crystals to construct the inter-crystalline boundary. Taking for instance two-dimensional crystals placed freely in the space, which can be viewed as a cross-section of a three dimensional crystal film parallel to the substrate, a side of a crystal can have more than one neighbour. This increasing topological complexity is the reason why this problem is presently unsolved for the three-dimensional case of the model.

To circumvent the difficulties resulting from the topological complexity, a level set formulation of the problem as given by G. Russo and P. Smeraka [6] can be used. This formulation uses smooth functions on a finite grid to create an approximation of the model. This grid based approach has the advantage that the move from a two dimensional model to a three-dimensional model is straightforward, because the dimension of the grid, the functions and the interface conditions need to be extended; the data structure, however, remains unchanged. On the other hand, this approach has the drawback that we get a smooth solution and smooth corners in contrast to a solution found by a constructive method which includes sharp edges. We can neglect these artefacts of the approximation, if we use a fine grid, but this automatically leads to a larger memory footprint. Using the working memory in an

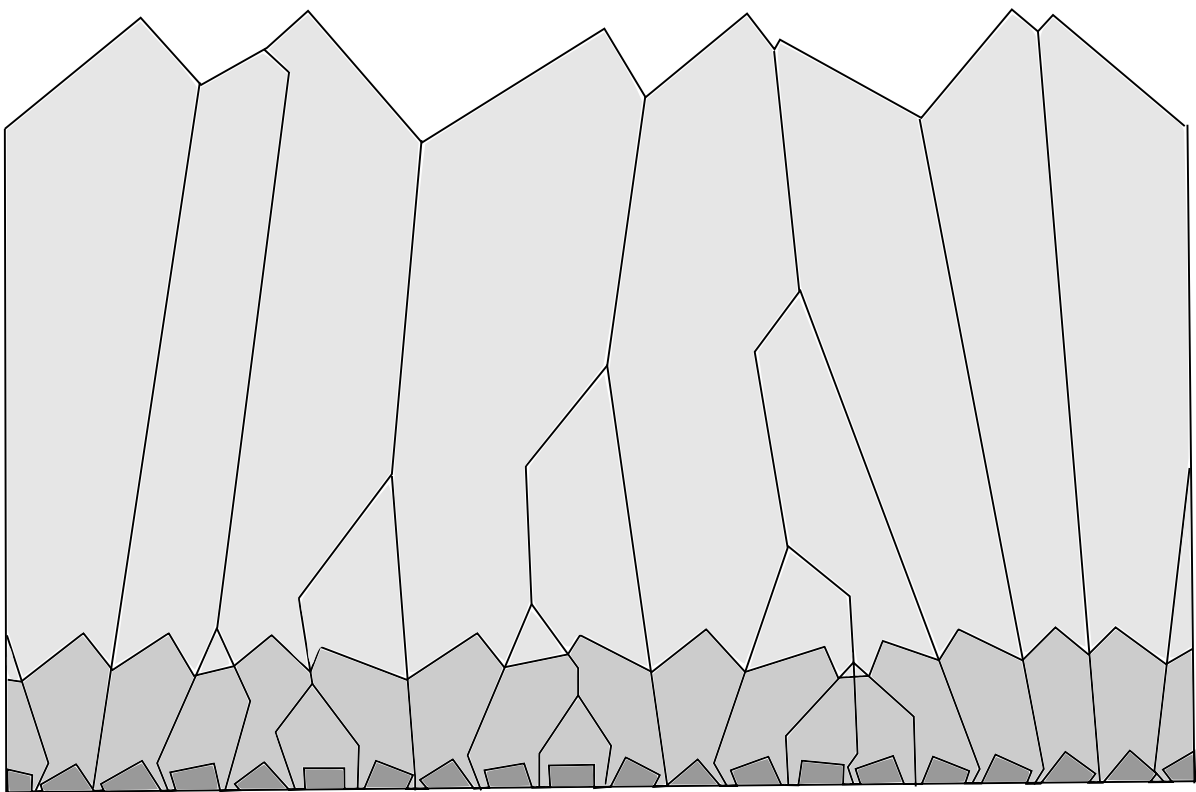


Figure 3.1: Example for the Van der Drift Growth Model

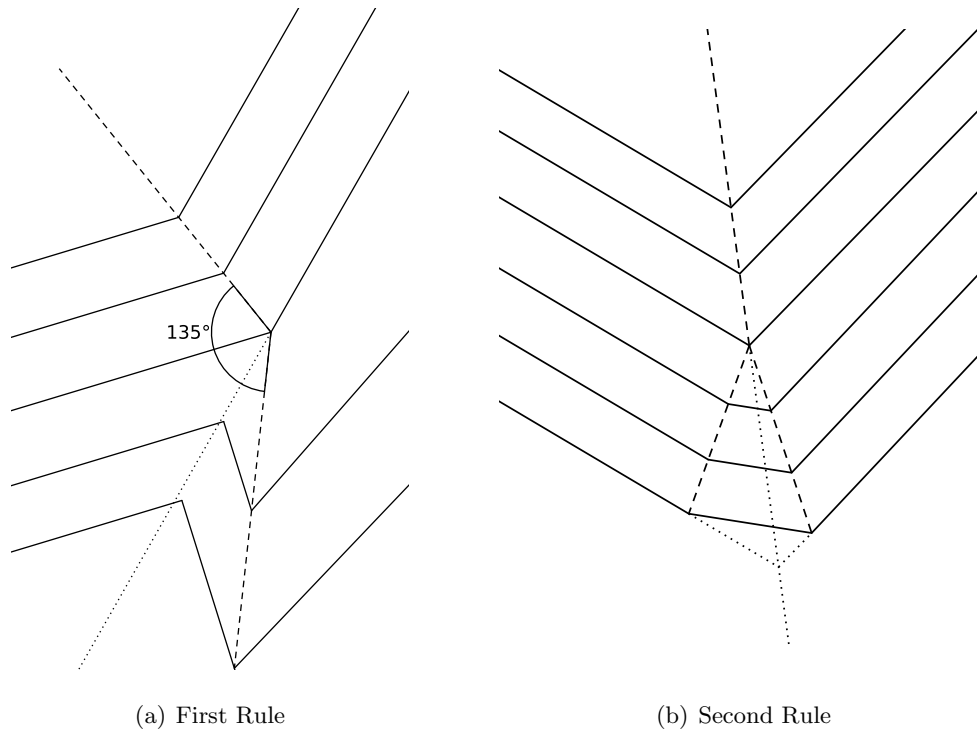


Figure 3.2: The Two Growth Rules Used by Van der Drift

efficient way by writing the inactive parts of the grid to the disk and only looking at the active narrow band of the crystals, they were constrained to a grid of $350 \times 350 \times 1200$ and 200 level-set functions on a machine with 1 GB of memory [20]. This approach gives good results and the precision and the number of crystals can be increased as more memory is now available and being a grid based approach, the algorithm can be parallelized. However, such an increase rapidly reaches the limits of available computing power.

3.1 Possible Events on a Crystal Side

In this section we look at the different events which can happen on a crystal side. On this information we build our algorithm, which, in contrast to a grid-based approach, does not suffer from the problem of a large memory footprint and is more flexible than a vertex tracking approaches, e.g. [21]. Rather than a vertex tracking approach, we use a side tracking approach and the vertices are properties of the sides and are only used for drawing and exporting purposes. The construction rules used by Van der Drift require the use of neighbour information prior to a formation of a new boundary. As mentioned at the beginning of this chapter, this topological information is difficult to gather, therefore, we seek to avoid its use. For this reason we reformulate the rules to a single simpler one. Looking at figure 3.2 we see that the inter-crystalline boundary, which is visualized by the dashed lines, consists of the trace of the intersection points of the two crystals. Since the sides of the

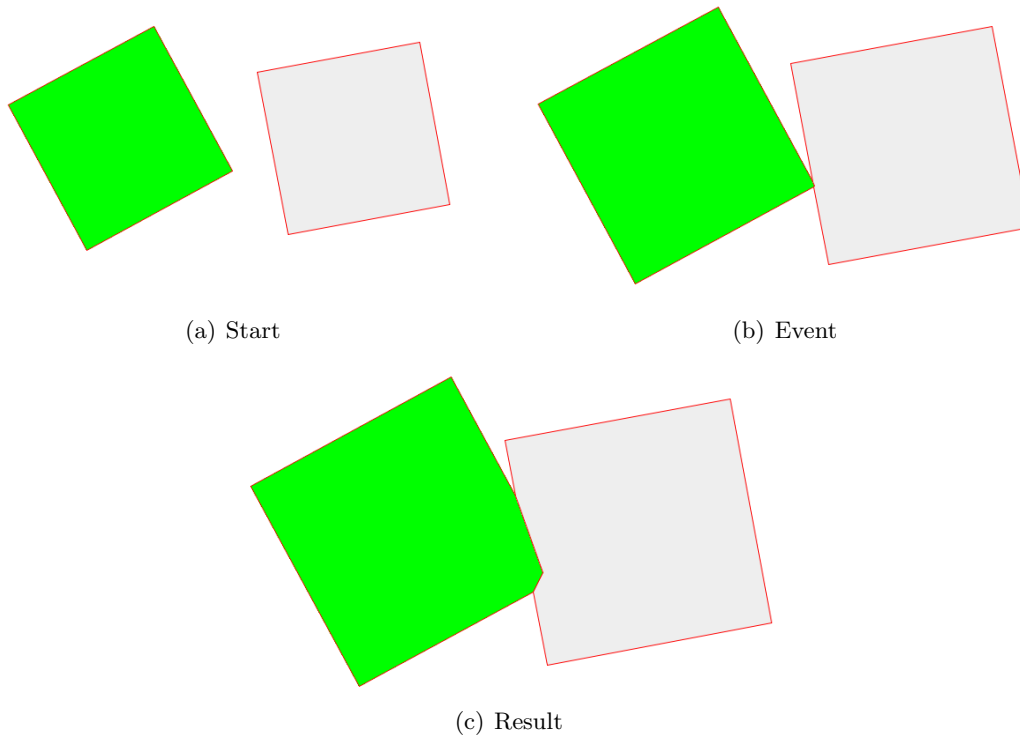


Figure 3.3: Vertex Hits Side

crystals grow in a linear fashion, the trace is also linear. Therefore, it suffices to calculate two of the intersection points to construct the boundary.

Another characteristic of our algorithm is that we use an event based approach. We react on an event happening on a side of a crystal and use these to build the inter-crystalline boundaries. Using such an event based approach leads to less topological information in our data structures and is close to a manual construction. A downside of this approach is the need for a time resolution which is fine enough to capture all events early enough to handle them in the right way. Additionally, the numerical nature can lead to instabilities result of certain singular events.

To handle the growth process using an event based approach we need to identify the different possible events. In this section we give a set of topological configurations sufficient for this purpose, including cases which can only arise in a more general case than the one shown in figure 3.1. For instance a two dimensional setting, which describes the growth of the bases of three dimensional crystals on the substrate.

3.1.1 Vertex hits Side

This event, shown in figure 3.3, gives rise to two actions on the sides of these crystals:

1. *Side Splitting* in the case of the grey crystal. This event results in the side being split with two inter-crystalline boundaries in the middle.

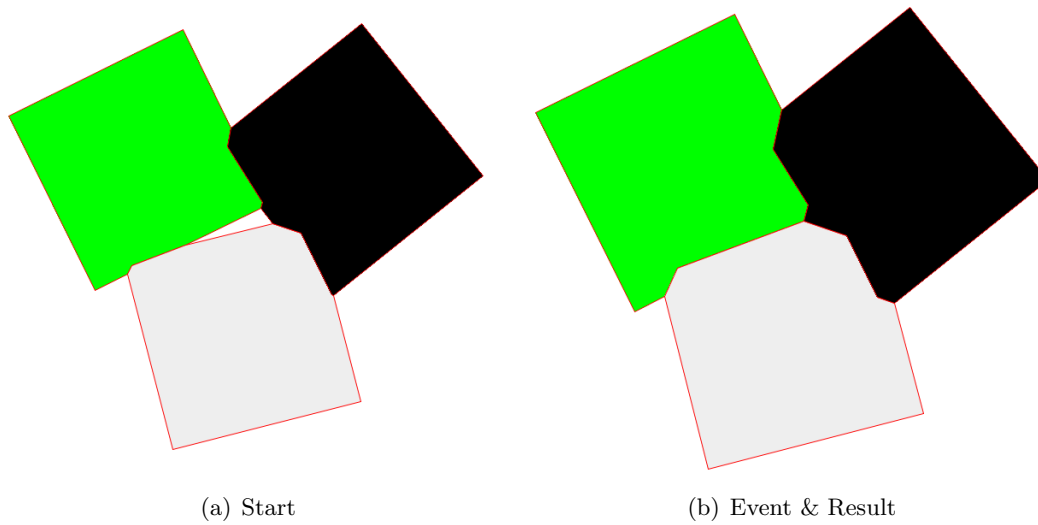


Figure 3.4: Fusion of Three Sides

2. *Softened Corner* in the case of the green crystal. This event results in the creation of two inter-crystalline boundaries beginning at the corner involved in the event. The term 'softened' stems from the fact that the angles created by the new inter-crystalline boundaries are greater than the angle of the edge before the event.

3.1.2 Fusion

In figure 3.4 a case of fusion is depicted, where three crystals are fused together. There are different possibilities with similar pictures involving more crystals. The event in the view of each of the three sides is called *Deletion*, because they vanish and only the inter-crystalline boundaries remain.

3.1.3 First Type of Overgrowth

In the figure 3.5 we see the green crystal overgrowing the grey crystal. The actions for this event are:

1. The action *Overgrown Edge* happens on the side of the grey crystal. This action results in a deleted side and a new inter-crystalline boundary of the neighbouring side with the green crystal.
2. In the case of the green crystal, the action *Overgrowing an Edge* is shown. In view of this crystal only a new inter-crystalline boundary is created.

3.1.4 Second Type of Overgrowth

Figure 3.6 shows the second type of overgrowth, where in contrast to the first type only three crystals are involved. The events are:

1. *Deletion* for the side of the grey crystal. Resulting in a deleted side.

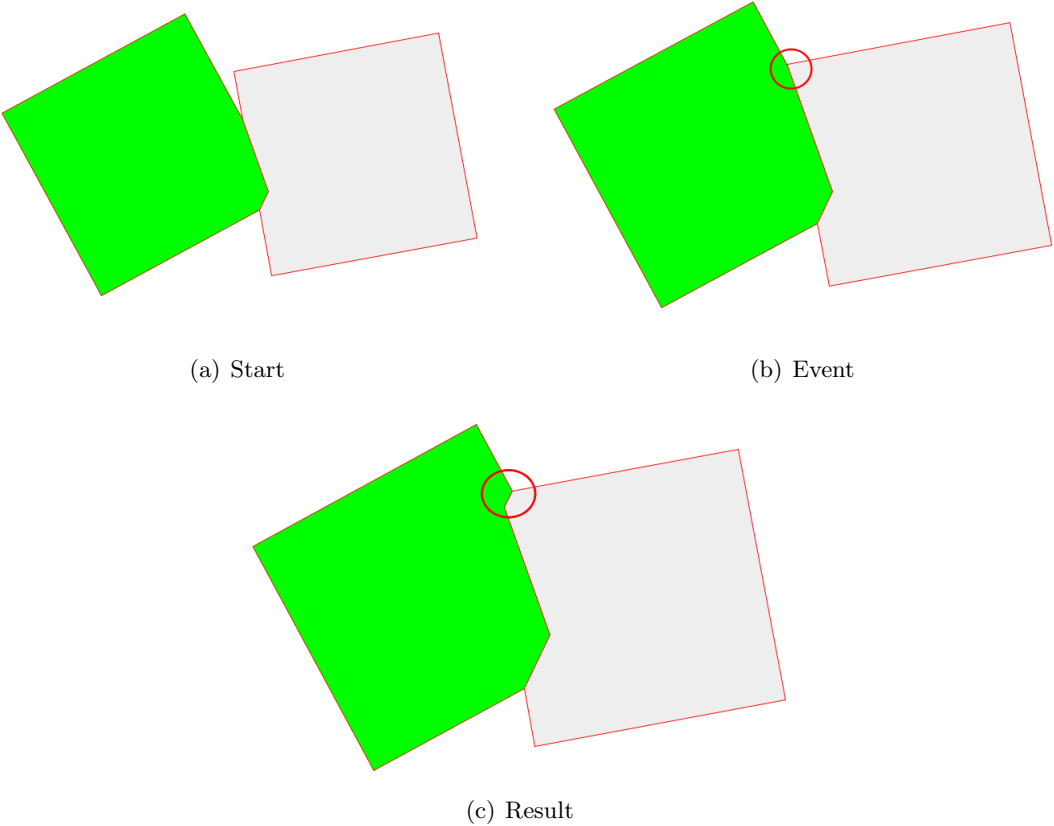


Figure 3.5: First Type of Overgrowth

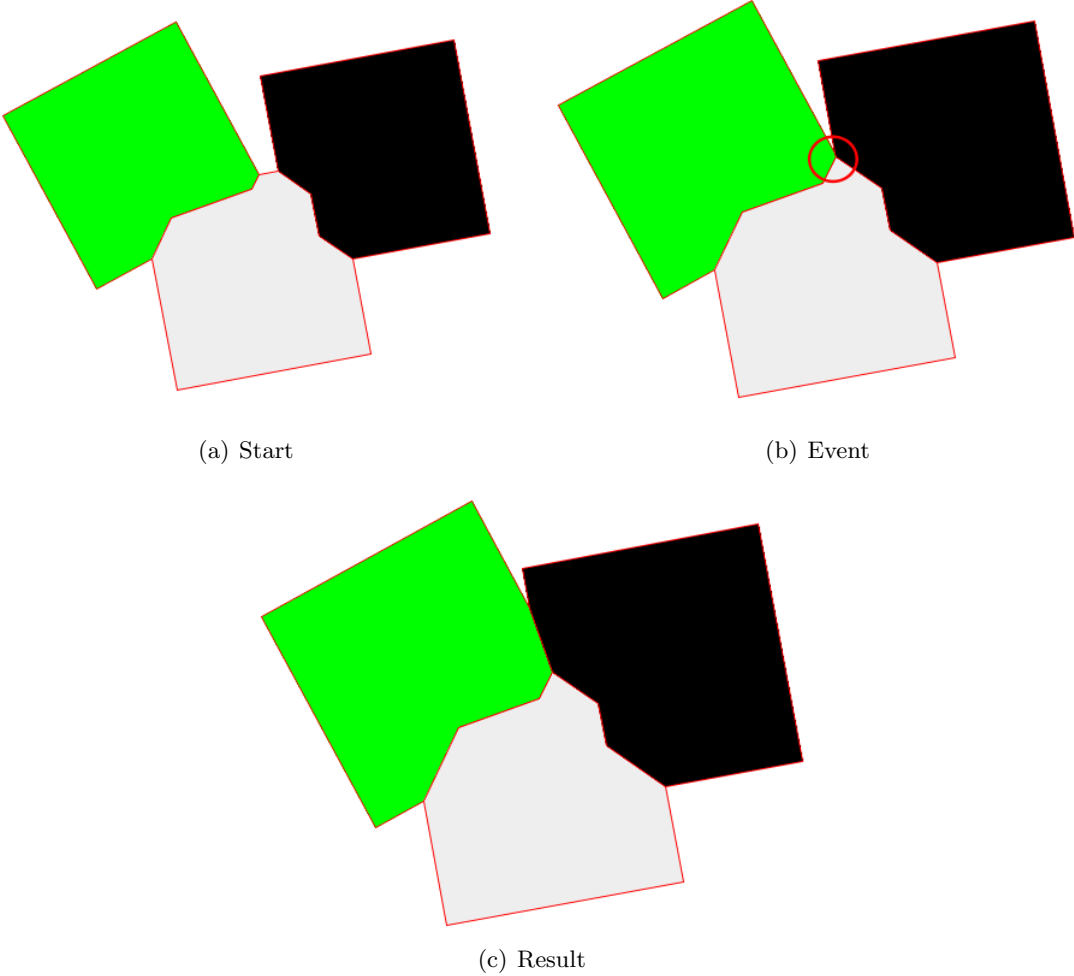


Figure 3.6: Second Type of Overgrowth

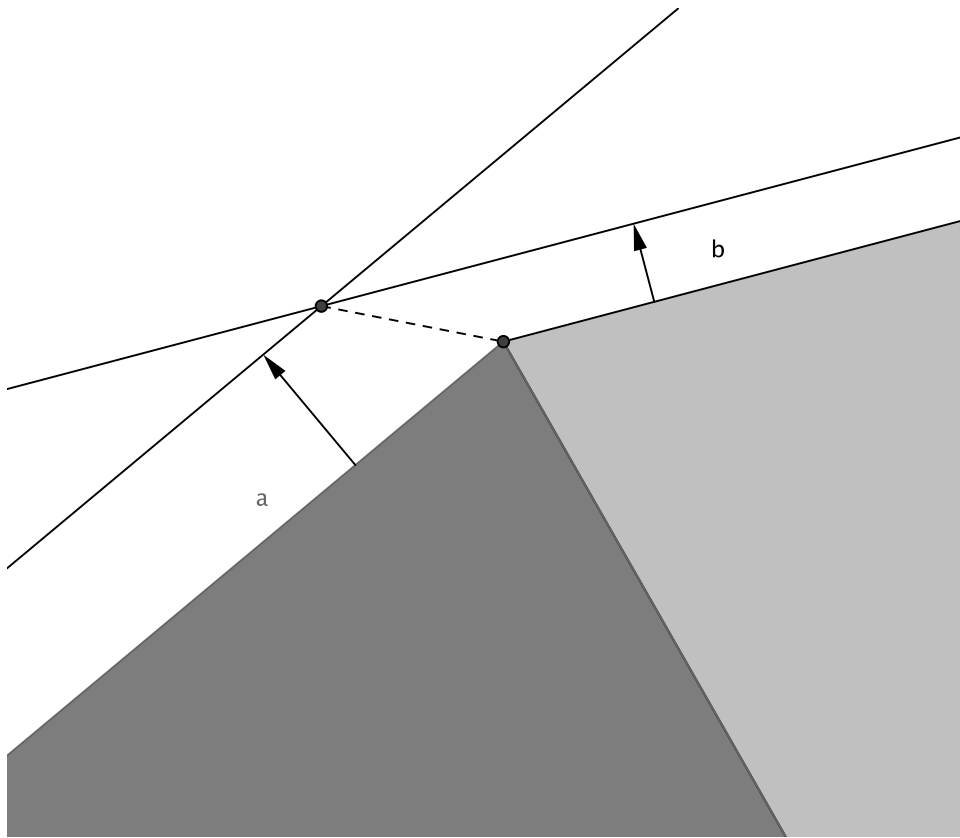


Figure 3.7: Model Problem

2. *Side hits Side* for the side of the green crystal. The action results in a new inter-crystalline boundary between the green and the black crystal.
3. *Side hits Side* for the black crystal. This action results in a new inter-crystalline boundary.

Additional topological configurations can arise in a simulation run. There are possibilities of more than three interacting crystals, but they are composed of the side events described.

The event based approach is versatile enough to handle other cases than the one of infinite surface diffusion, for example the case of infinite diffusion restricted to a crystal. For this case Van der Drift calculated the direction with maximum growth based on the difference in the normal speed. The dependence of the growth speed to the orientation poses no problem in the calculation of the maximum growth. However, given two sides with different growth speeds, the following situation can arise (see figure 3.7). Even though the side *a* grows faster than side *b* in figure 3.7 the side *a* shrinks and the side *b* gains size. There are two possible ways of avoiding this kind of problem:

1. Restricting the orientations of the crystals
2. Using the counter-intuitive result given by the trace of the intersections of the sides as depicted in figure 3.7. The dashed line in the figure shows the inter-crystalline

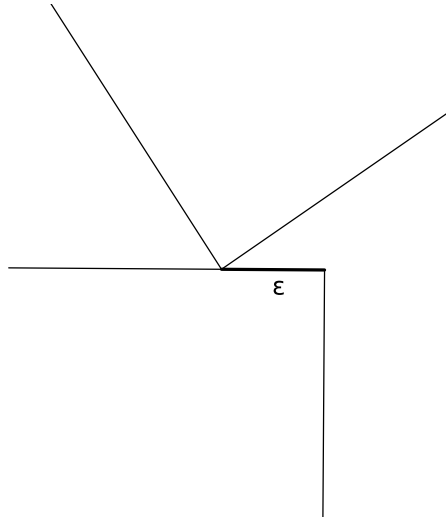


Figure 3.8: Small Side After Side Splitting

boundary that would be created. We see that because of the orientation of the boundary, the slower growing crystal will overgrow the faster one.

This is a weakness of the formulation and not of the model. A possible solution is to alter the growth speed by incorporating diffusion along the connected crystals. This is not straightforward and stands in conflict with the assumption of constant normal velocity, since the speed of normal growth would differ dependent on the sides surrounding it, describing a model which is different to the Van der Drift model considered.

3.2 Identification of Events

Knowing the different events which can arise during a simulation run is not enough for an implementation of the algorithm. The events have to be identified to be handled in the way described in the previous section.

3.2.1 Side Splitting or Softened Edge

These actions are easily identified by the presence of two new intersections for a side or an edge respectively.

3.2.2 Deletion

A naive approach is to iterate over all sides and delete the ones smaller than a certain threshold. There are two reasons this straightforward method cannot work. First, the situation in figure 3.8 can arise which shows the creation of a small side by a hit of a another crystal. This small side is not certain to vanish.

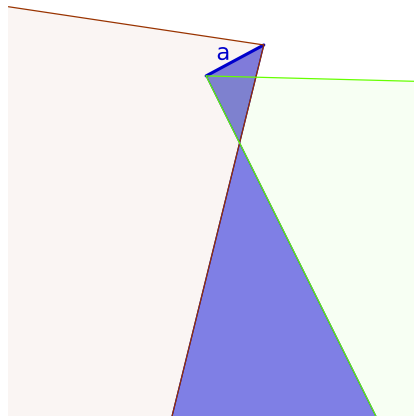


Figure 3.9: Missed Deletion

Second, the time-steps where the length is smaller than the minimum (see figure 3.9) could be missed.

There are two possibilities to deal with this: One is to calculate the time the side will vanish using the length difference of two time-steps. This works, because all interacting entities are of linear nature. The disadvantage is that the prediction has to be changed every-time another crystal interacts with the side.

A more elegant way is to use the outcome of a missed deletion in figure 3.9 as a way of identification. If a deletion is missed, the normal vector calculated using the beginning and the end of the line points in the opposite direction to the normal of the line, which it otherwise does not.

3.2.3 Side hits Side

This action is triggered by a new boundary between two previously unconnected crystals.

3.2.4 Overgrown Edge or Overgrowing an Edge

At the beginning, two crystals are connected with an inter-crystalline boundary (see figure 3.5). One of the adjacent sides of this boundary is deleted and the edge lies on the inter-crystalline boundary. The first possible solution is to intersect each line of both crystals at every time-step and detect new intersection points. As soon as the edge lies on the inter-crystalline boundary, we get a new intersecting point. But because of the nature of the problem, we will always miss the exact time-step, therefore we need to include a tolerance for accepting the points (see figure 3.10). The problem with this approach is to find the right value for this tolerance. If set to low, we miss crystal overgrowth and if we set it to high, we get false results.

Looking at figure 3.10, we notice that the boundary line of the crystal in light grey is longer than the boundary line of the dark grey crystal. This can only be a result of overgrowth and is not a possible result of the simulation, since inter-crystalline boundaries are not visible on the surface. Therefore, this second strategy is the better way of identification.

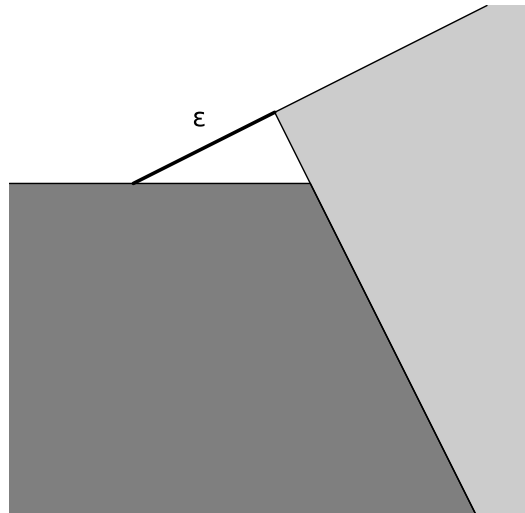


Figure 3.10: Overgrowth Problem

3.3 Technical Implementation

This section gives an overview over the technical implementation of the algorithm used for the simulations. First, we look at the program flow, which reveals the implicit assumption that only one event happens at each time-step. If this was not the case, the order of the tests for the events could influence the simulation outcome. By the right choice of time-step size this should pose no problem.

The structure of the program as we see in figure 3.11 is almost serial. The conditional flow breaks the otherwise serial nature and has furthermore the most potential for errors, because it relies on the numerical results of the test for intersections. This is the Achilles heel of this algorithm, but this is a numerical problem common in graphical algorithms and difficult to solve [25].

The structural overview of the implementation shows the connections of the different classes used in the program. The main class is `Crystal Configuration`, used for administration of the crystal growth on the substrate and, therefore, is the root of figure 3.12. Other than this class, three different graphical classes exist in the program.

At every time-step, the `bounding box` of the crystals is cached and used in the main class to improve the speed of the intersection tests. The performance gain is significant, because for the intersection of two bounding boxes only comparisons are needed, whereas the intersection of the crystals themselves need multiplications and divisions in addition to comparisons to be performed.

The instance of the `polygon` class is used in the main class for the borders which limit the simulation vertically and horizontally. These borders need to be intersected with all of the crystals and therefore the bounding box class is part of this class for speed-up.

In contrast, the `polygon` in the `crystal` class are used to get the intersection points of two crystals. The polygon represents the crystal growing in its starting shape without the interaction with other crystals. This simplifies and speeds up the process, as otherwise all instances of a side created through splitting by other crystals have to be handled separately.

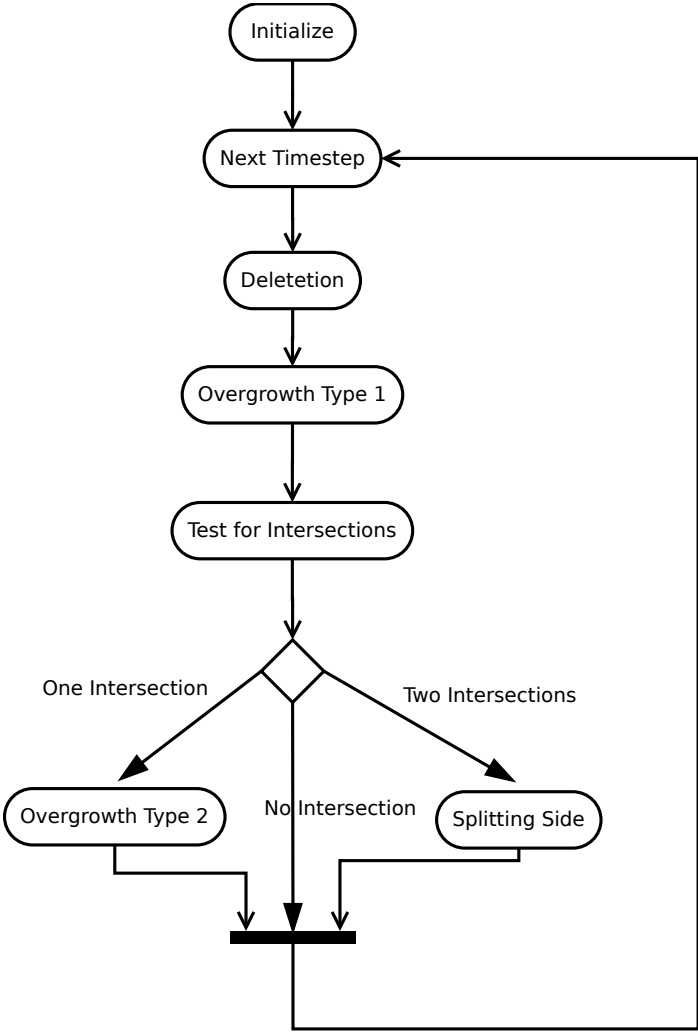


Figure 3.11: Program Flow

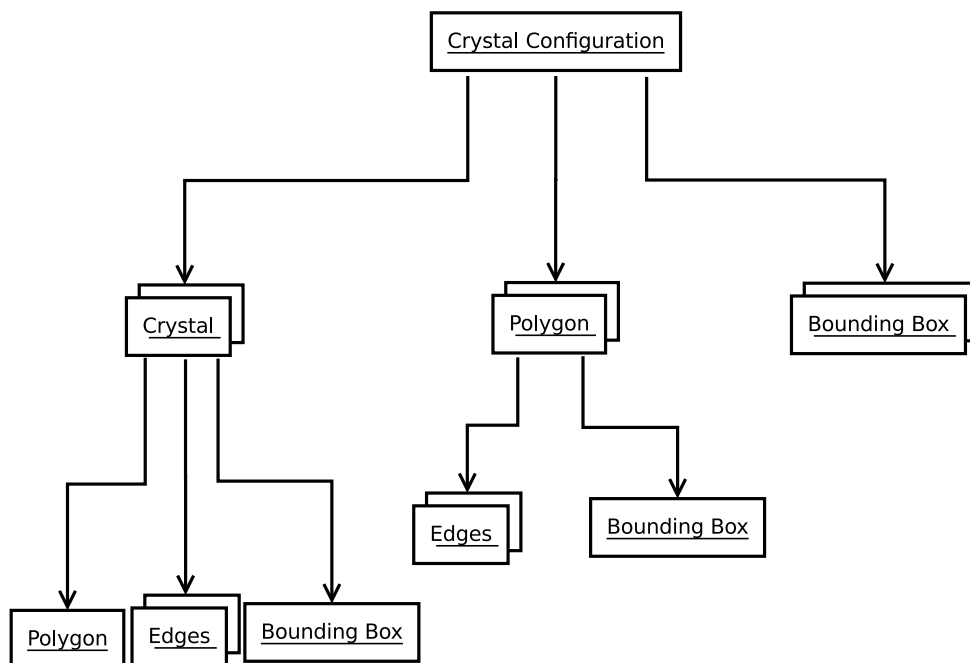


Figure 3.12: Program Structure

Chapter 4

An Extension of the Van der Drift Model

In this chapter, we look at the restriction or the partial restriction of the surface diffusion to a crystal. In addition to the derivation of the orientation of maximal speed, the orientations admissible for simulations are investigated.

4.1 Surface Diffusion Restricted to a Crystal

In this case we assume that infinite surface diffusion is restricted to the crystals instead of the whole film. Because the material is not distributed evenly along the whole film, the normal growth speed of two crystals differs depending on the amount of material collected. The amount varies because of the surface and the orientation of its sides. This has been investigated by Van der Drift [1] in the case of needles. However, needles are with respect to their growth one-dimensional. For two-dimensional simulations, an angle dependent growth rate for a right-angled triangle is derived, for which the maximum growth speed and the admissible angles for the material are calculated.

In the following we assume that the amount of deposited material is one unit for a line of length one, which is perpendicular to the direction of the incoming material.

Lemma 3. *If the angle between the needle and the substrate is θ and the orientation of the incoming material is θ' , then the amount of material collected by a needle is*

$$\sin |\theta' - \theta| \tag{4.1}$$

per unit length.

Proof. Looking at the figure 4.1, we see that m , the amount of material coming in orthogonal direction, is $\sin |\theta' - \theta|$ times the amount of material which in our case is 1. \square

Although the case is simple, it is related to the case of right-angled triangles, which can be viewed as two needles in terms of material gathering.

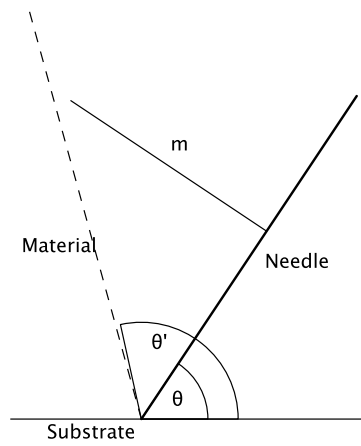


Figure 4.1: Needle

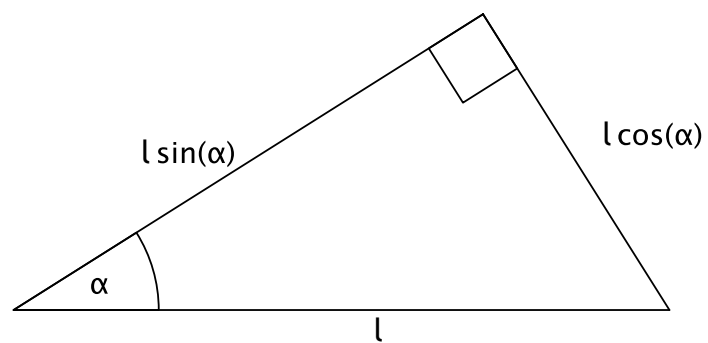


Figure 4.2: Surface of a Right-Angled Triangle

Theorem 3 (Growth Speed of a Right-Angled Triangular Crystal). *Given the angle of the incoming material θ , the angle α of the crystal and assuming the lateral size of the crystal to be l , we get for the normal velocity v of the edges with the proportionality factor v_0 :*

$$v = \frac{\max(\sin(\theta - \alpha), 0) \cos \alpha + \max(\cos(\theta - \alpha), 0) \sin \alpha}{\sin \alpha + \cos \alpha} v_0, \quad (4.2)$$

or in different form:

$$\begin{aligned} \theta > \frac{\pi}{2} + \alpha : & \quad v = \frac{\sin(\theta - \alpha) \cos \alpha}{\sin \alpha + \cos \alpha} v_0, \\ \alpha \leq \theta \leq \frac{\pi}{2} + \alpha : & \quad v = \frac{\sin \theta}{\sin \alpha + \cos \alpha} v_0, \\ \theta < \alpha : & \quad v = \frac{\cos(\theta - \alpha) \sin \alpha}{\sin \alpha + \cos \alpha} v_0. \end{aligned}$$

The vertical growth rate h of the crystals is

$$h = v (\sin \alpha + \cos \alpha).$$

Proof. Looking at figure 4.2, we see that the amount of material collected by the two edges is $l \cos \alpha \max(\sin(\theta - \alpha), 0)$ and $l \sin \alpha \max(\cos(\theta - \alpha), 0)$. This material is distributed evenly along the surface of the crystal, which is $l \sin \alpha + l \cos \alpha$. Putting this together we get the first part of the theorem.

For the second part, we look at the cases where one of the maxima is less than zero.

The third is an application of the corollary 4. \square

Corollary 5 (Maximum Vertical Growth Rate of a Right-Angled Triangular Crystal). *Given the angle θ of the incoming material, the maximum vertical growth rate v_{\max} and the angle α of maximum growth are:*

$$\begin{aligned} \theta > \frac{\pi}{2} : & \quad \alpha = \frac{\theta}{2} - \frac{\pi}{4}, \\ & \quad v_{\max} = \sin\left(\frac{\theta}{2} + \frac{\pi}{4}\right) \cos\left(\frac{\theta}{2} - \frac{\pi}{4}\right) v_0, \\ \theta = \frac{\pi}{2} : & \quad v_{\max} = \sin \theta v_0, & \quad \text{For every } \alpha. \\ \theta < \frac{\pi}{2} : & \quad \alpha = \frac{\theta}{2} + \frac{\pi}{4}, \\ & \quad v_{\max} = \cos\left(\frac{\theta}{2} - \frac{\pi}{4}\right) \sin\left(\frac{\theta}{2} + \frac{\pi}{4}\right) v_0, \end{aligned}$$

where v_0 is the proportionality factor of the growth speed.

Proof. If we remove the the maximum function from (4.2) in theorem 3, we note that the growth rate equals:

$$\frac{\sin \theta}{\sin \alpha + \cos \alpha} v_0. \quad (4.3)$$

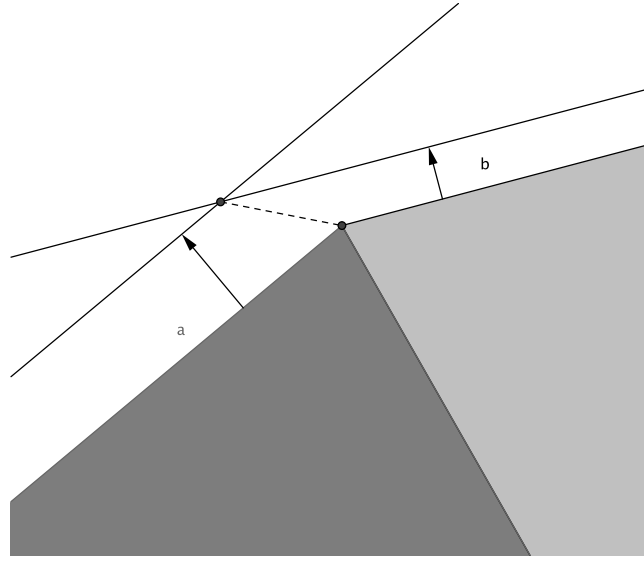


Figure 4.3: Model Problem

In this case the vertical growth rate is $\sin \theta v_0$ independent of the angle α of the crystal. The removal of the maximum function made the value smaller, hence if the contribution of a side of the crystal is negative, the contribution of the other is greater than $\sin \theta$, which is the sum of both. So we separately look at the collection of the two sides, which in conjunction with differentiation gives us the result. \square

The calculation of the growth speed of a given triangle allows a simulation. However, we have to ascertain that a case similar to the one shown in figure 4.3 cannot arise, where even though the growth speed of the side a is greater than that of side b , the inter-crystalline boundary given by the model makes the side a smaller with every time step. This can happen, because in contrast to the previous case, a left-oriented crystal can overgrow a right-oriented crystal and vice versa. This can be avoided by ensuring that the vertical growth of a side of a crystal is less than the vertical growth of the top of crystal, regardless of its orientation.

Lemma 4 (Admittable Material Deposition Angles). *A starting configuration consisting of right-angled triangular shaped crystals and assuming infinite surface diffusion restricted to each crystal does not suffer from the model problem shown in figure 4.3 if the angle θ of incident material is in the interval $[\frac{1}{4}\pi, \frac{3}{4}\pi]$.*

Proof. $\theta \geq \frac{\pi}{2}$: For $\theta > \frac{\pi}{2}$, the ray of material comes from the left hand side, therefore the side which collects the most material is on the left side of the triangle. Hence the maximum growth m of side fulfils the following equation:

$$m(\alpha) = \frac{\sin(\theta - \alpha) \cos \alpha}{\sin \alpha + \cos \alpha} v_0. \quad (4.4)$$

The minimal vertical growth for a crystal in the configuration is $\sin \theta v_0$. The problematic case can only arise if the vertical growth of the side is greater than the minimal verti-

cal growth for a whole crystal. Extracting the vertical component of m , which equals a multiplication by $\cos \alpha$, we can compare the two growth speeds:

$$g(\alpha, \theta) = \frac{\sin(\theta - \alpha) \cos^2 \alpha}{\sin \alpha + \cos \alpha} - \sin \theta. \quad (4.5)$$

The function g is smaller than zero if θ is $\frac{\pi}{2}$ regardless of the choice of α . As the function is smooth, its value is zero before it becomes positive and simulation is not possible. For this reason we equate the points where the function is zero.

$$g(\alpha, \theta) = 0 \quad (4.6)$$

$$\Leftrightarrow \sin \theta = \frac{\sin(\theta - \alpha) \cos^2 \alpha}{\sin \alpha + \cos \alpha} \quad (4.7)$$

$$\Leftrightarrow \sin \theta = \frac{(\sin \theta \cos \alpha - \cos \theta \sin \alpha) \cos^2 \alpha}{\sin \alpha + \cos \alpha} \quad (4.8)$$

$$\Leftrightarrow 1 = \frac{\cos^3 \alpha - \sin \alpha \cos^2 \alpha \frac{\cos \theta}{\sin \theta}}{\sin \alpha + \cos \alpha} \quad (4.9)$$

$$\Leftrightarrow -\cot \theta = \frac{\sin \alpha + \cos \alpha - \cos^3 \alpha}{\cos^2 \alpha \sin \alpha} \quad (4.10)$$

$$\Leftrightarrow \tan \theta = -\frac{\cos^2 \alpha \sin \alpha}{\sin \alpha + \cos \alpha - \cos^3 \alpha} \quad (4.11)$$

$$\Leftrightarrow \theta = \tan^{-1} \left(-\frac{\cos^2 \alpha}{\sin \alpha \cos \alpha + 1} \right) \quad (4.12)$$

Looking at first derivative of this equation

$$g'(\alpha, \theta) = \frac{\cos \alpha (\cos \alpha + 2 \sin \alpha)}{-\cos^4 \alpha + \cos^2 \alpha + 2 \sin \alpha \cos \alpha + 1}, \quad (4.13)$$

we see that it is positive because $\sin \alpha$ and $\cos \alpha$ are positive as $\alpha \leq \frac{\pi}{2}$. Therefore, we get the minimal θ for $\alpha = 0$ and $\theta \leq \frac{3}{4}\pi$.

The second case follows because of symmetry. \square

For the growth rule to hold, we have assumed a constant ratio of the sides of a crystal, which are allowed to vary during a simulation. However, these restrictions are imposed by the use of the Van der Drift model which uses constant velocities.

The use of right-angled triangles for this case is reasonable, because if squares would be used the question of the influence of the downward orientated sides would have to be dealt with.

4.2 Surface Diffusion Partially Restricted to Crystals

Lemma 5 (Admittable Material Deposition Angles). *A starting configuration consisting of right-angled triangular shaped crystals assuming infinite surface diffusion partially restricted to each crystal does not suffer from the model problem shown in figure 4.3 if the angle θ of incident material is in the interval $[\frac{1}{4}\pi, \frac{3}{4}\pi]$.*

Proof. Let m_1 be the material diffused only on the crystal and m_2 the material distributed along the film. The angle α is the angle of the triangle threatening the overgrowth and α_1 the angle of the other triangle. For making sure that the situation depicted in figure 4.3 can not happen we use a proof similar to the one of lemma 4 and compare the vertical growth of the two triangles.

$$m_1 (\cos \alpha - \sin \alpha_1 - \cos \alpha_1) + m_2 \left(\frac{\sin (\theta - \alpha) \cos^2 \alpha}{\sin \alpha + \cos \alpha} - \sin \theta \right) \geq 0. \quad (4.14)$$

As we see the two influences of the growth speed can be readily separated. Therefore, we only have to deal with the new one. However, this turns out to be simple, as $\cos \alpha \leq \sin \alpha_1 + \cos \alpha_1$ regardless of the angle α_1 :

$$\sin \alpha_1 + \cos \alpha_1 \geq 1 \quad (4.15)$$

$$\Rightarrow \underbrace{\sin^2 \alpha_1 + \cos^2 \alpha_1}_{=1} + 2 \sin \alpha_1 \cos \alpha_1 \geq 1 \quad (4.16)$$

Since all quantities are positive and therefore the square is a monotone function, the proof is complete. \square

Chapter 5

Simulation

In this chapter the results of the simulations are presented, which are using an implementation of the algorithm discussed in the previous chapter. First we look at the classical example of the Van der Drift model using an initial configuration consisting of squares of equal size and the equivalence to a case consisting of right-angled triangles in regard to the average in-plane crystal size. Both results are then compared to the theoretical result regarding the growth rate of such a setting.

5.1 Infinite Surface Diffusion on the Film

Since we assume infinite surface diffusion, any differences of the amount of material a crystal collects are evened out. For the classical example of the Van der Drift model, we start with squares of equal size, but different orientations. Two distinct distributions for the orientations of the square crystals are used: an uniform distribution and a normal distribution, cut off to stay in the interval of the possible cases (zero mean and variance equal half the size of the interval). The orientations of the crystals lie in the interval $[-\pi/8, \pi/8]$ and the sample size for the first simulations is 40 crystals.

The number is limited by problems of the graphical algorithm arising from the vertices on the side of the squares. These vertices can come very near to hitting each other, making it difficult for the algorithm to determine the side which is spilt. These problems become significant as the size of the crystals gets smaller, and with it the difficulty of choosing the right course of action increases. In figures 5.3 and 5.4 we see that the decrease of the number of crystals in the simulation is in agreement with our theoretical findings.

The equivalence regarding the growth rate, which we proved for the configuration consisting of right-angled triangles, exhibits itself in figures 5.5 and 5.6. The growth rate is as before proportional to \sqrt{t} . However, in comparison to the previous setting, the vertices on the sides now lie on the substrate and are handled - as termed in the description of the algorithm - as second type of overgrowth. For this reason an increase of the number of crystals to 100 is possible. The number is limited by the proper identification of the first type of overgrowth. A threshold of the length difference of constant sides is used, but depending on the sides involved a higher or a lower value is appropriate. Currently, a constant value is set. This can lead to mishandling of overgrowth, especially if the simulation involves interaction of crystals of largely varying size.

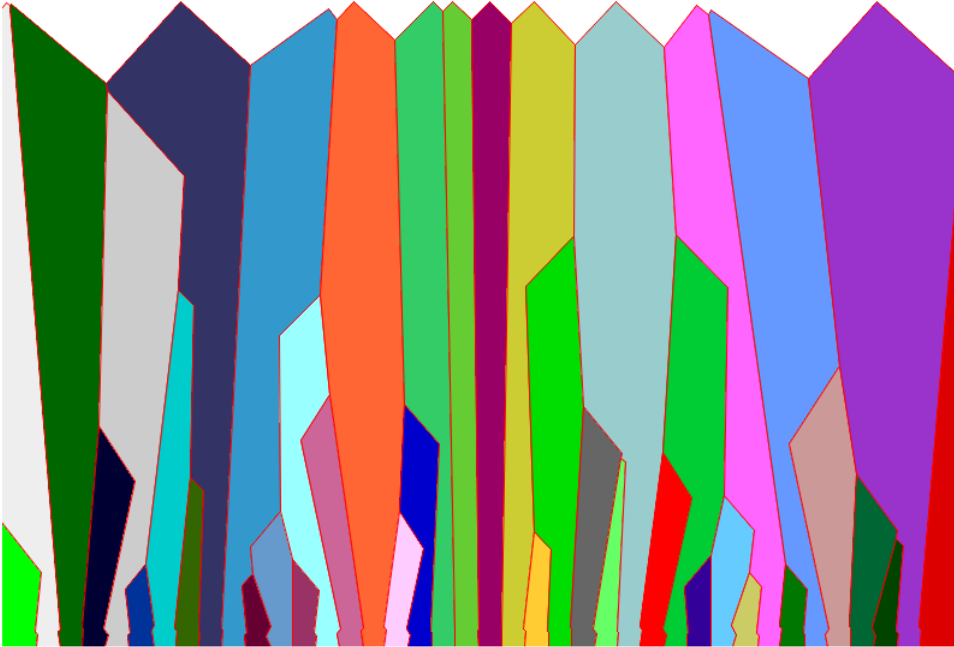


Figure 5.1: Simulation Results Starting with Squares

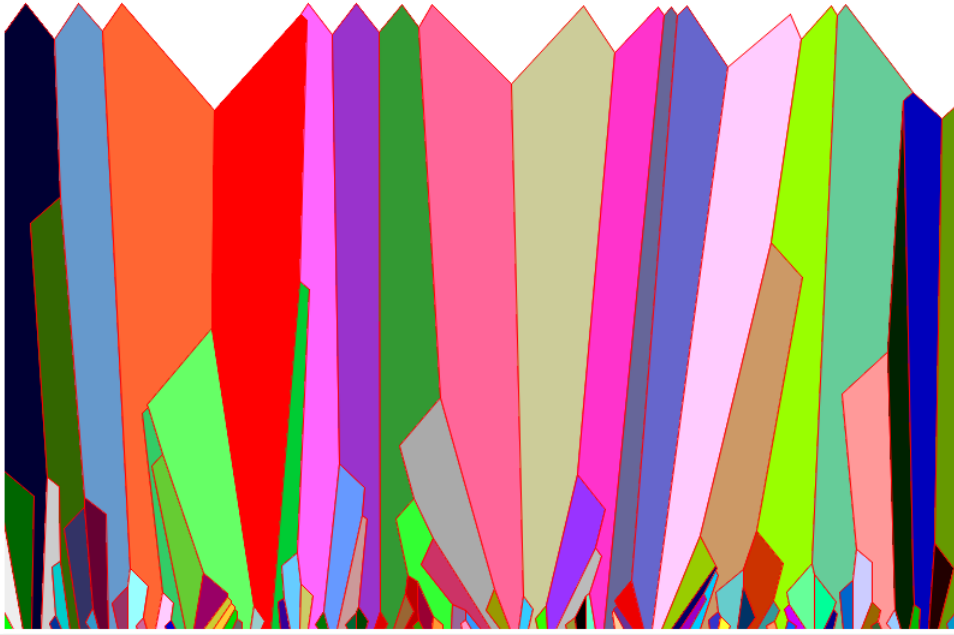


Figure 5.2: Simulation Results Starting with Right-Angled Triangles

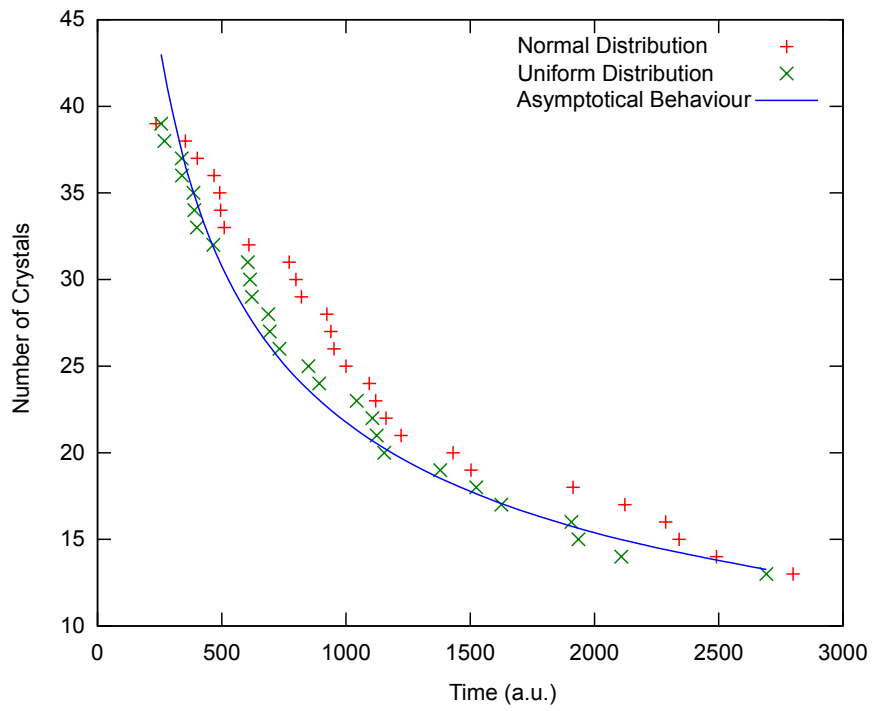


Figure 5.3: Number of Square Crystals over Time

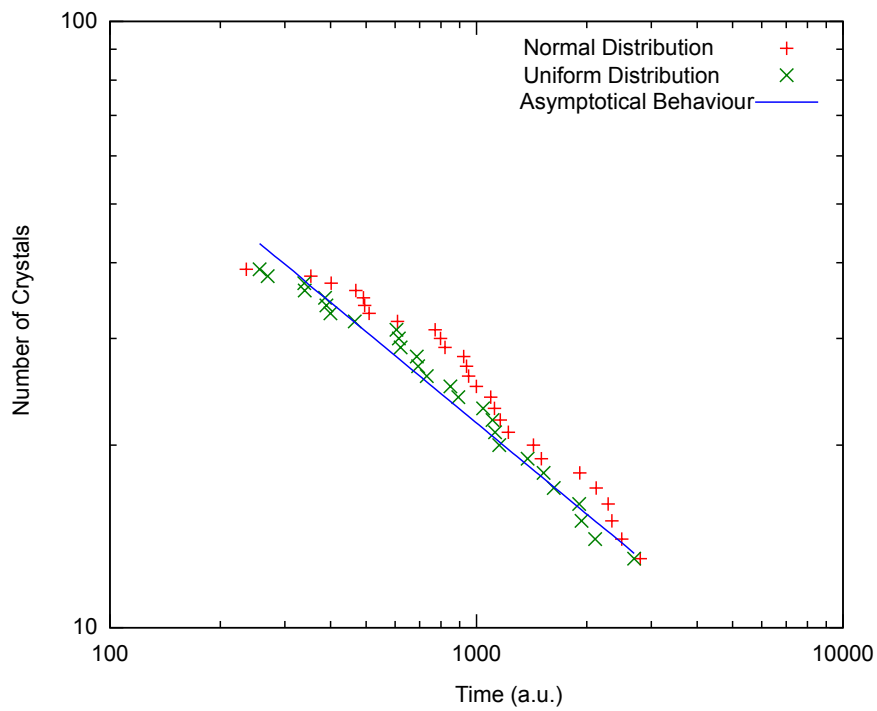


Figure 5.4: Number of Square Crystals over Time (Logarithmic Scales)

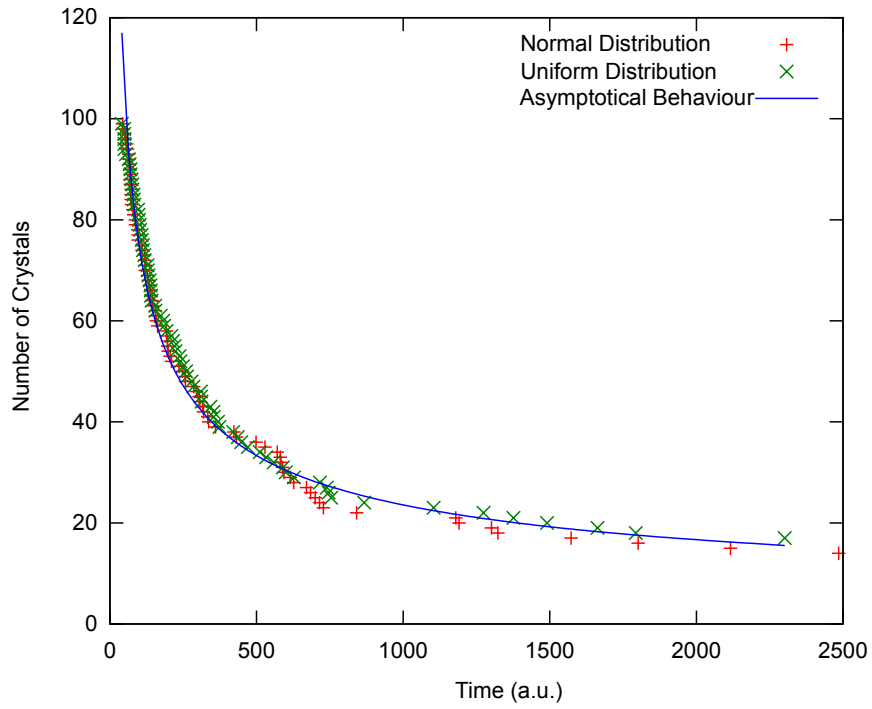


Figure 5.5: Number of Right-Angled Triangular Crystals over Time

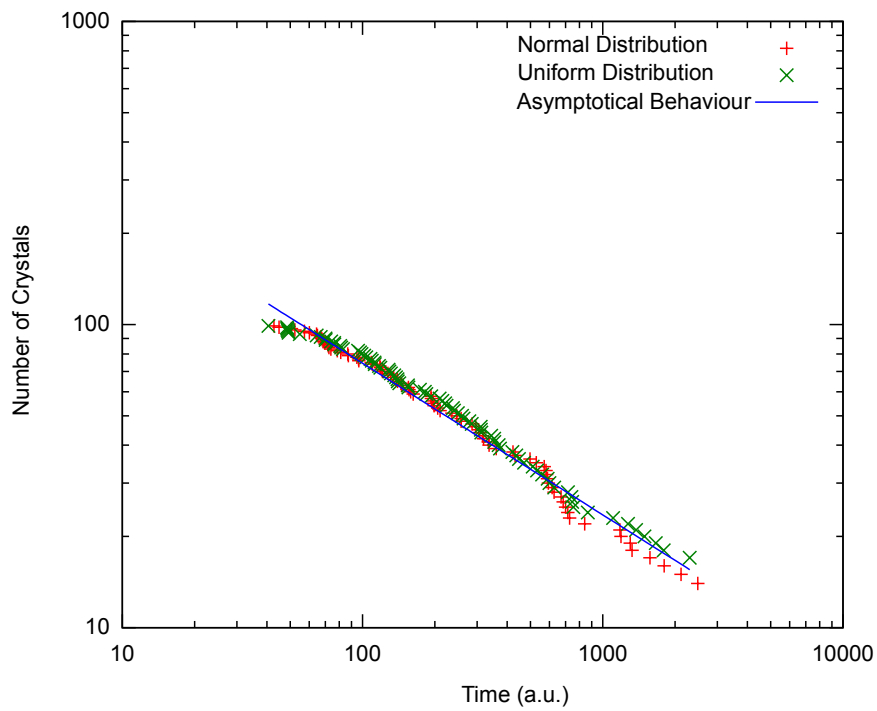


Figure 5.6: Number of Right-Angled Triangular Crystals over Time (Logarithmic Scales)

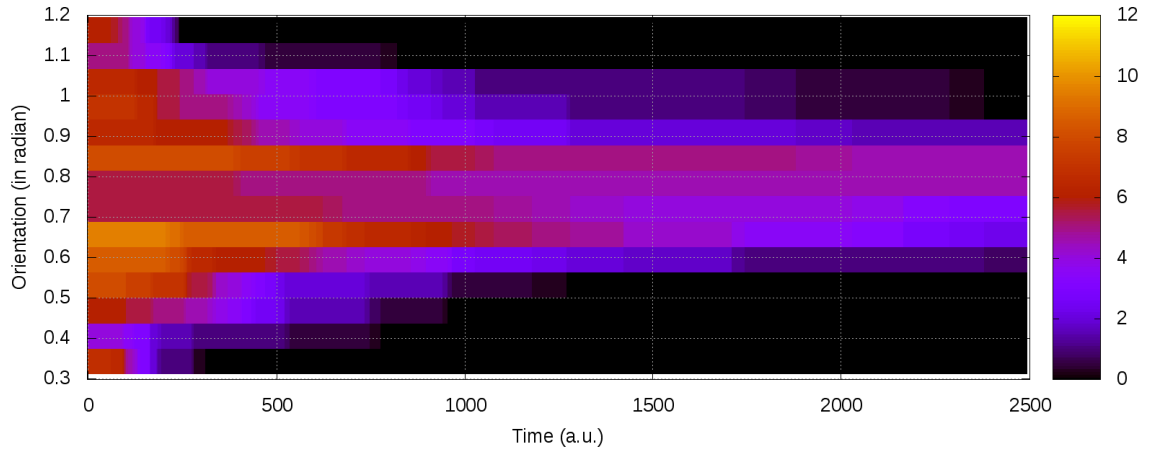


Figure 5.7: Remaining Angles Starting with a Uniform Distribution

In figure 5.7 the distribution of the angles of the triangles are shown, which survived until the current time-step. The angles are separated into 15 groups of equal size. The rapid decline of the unfavourable orientations is clearly visible with the rest resembling a log-normal distribution.

Comparing the two results (see figure 5.1, 5.2), the only visible difference is the kink in the film near the substrate if we start with squares. Up to this level the bottom sides of the squares play a part in the simulations which shows how little the influence of these sides on the simulations is.

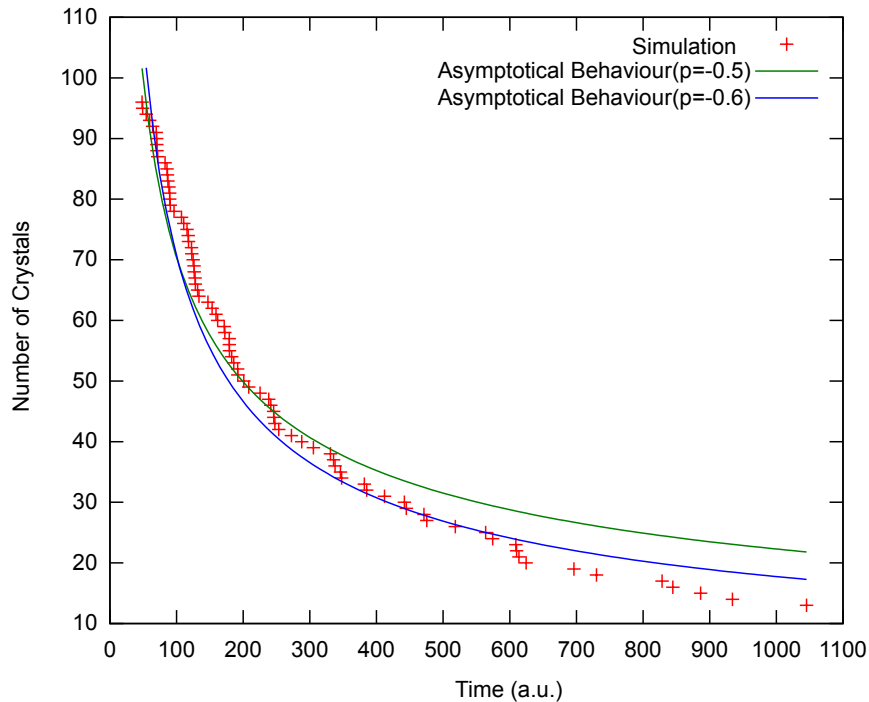


Figure 5.8: Number of Crystals over Time ($\theta = 0.7\pi$)

5.2 Infinite Surface Diffusion Restricted to a Crystal

If the assumed infinite surface diffusion is restricted to a crystal, the material each crystal collects becomes an important part of the survival. This amount is dependent on the angle of incidence and the surface of the crystal. This case has been investigated in terms of the orientation of maximum speed for the case of a needle by Van der Drift [1].

To emphasize the orientation of the surviving crystals, the angle is chosen near the admissible maximum. If for the case of material coming from the left, θ is chosen smaller than for example $\theta = 0.6\pi$, the maximum speed is reached by an angle of $\alpha = 0.05\pi$ and the vertical growth speed is $\sin\theta$ for all $\alpha \geq 0.1\pi$. Therefore, only a small percentage of the angles are influenced and only in the extremal regions for α , where computation becomes more difficult. For these reasons we look only at three cases: $\theta = 0.7\pi$, $\theta = 0.3\pi$ and $\theta = 0.5\pi$. The distribution of the angles chosen for the simulation is uniform and out of the interval $\alpha \in [0.1\pi, 0.4\pi]$.

In figures 5.8 and 5.9, we see that the growth rate for the crystal film does not clearly follow the power law proven for the case of infinite surfaces diffusion. It seems that a fit of the form $x^{0.6}$ is better, although looking at the logarithmic plot figure 5.13, it is dubious if a power law is followed at all.

The picture for the case of the material coming from the right (figure 5.10, 5.11) is similar to the one coming from the left. As the same sample of the angle distribution is used, we can see that the outcome of the previous simulation was not due to an overweight in the sample.

Next, three different choices of normal growth speed are compared (see figures 5.12, 5.13).

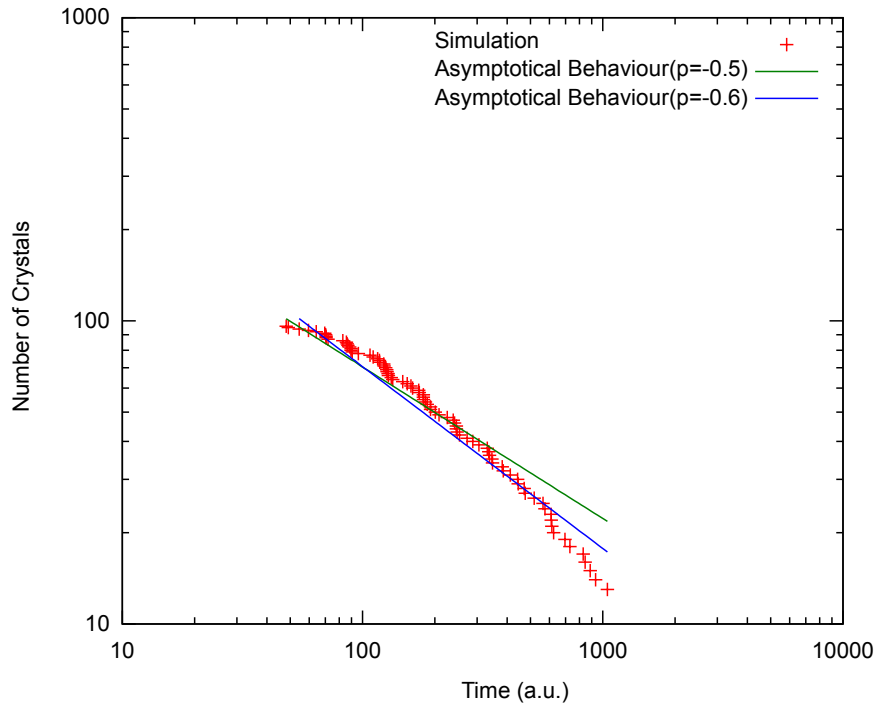


Figure 5.9: Number of Crystals over Time ($\theta = 0.7\pi$, Logarithmic Scales)

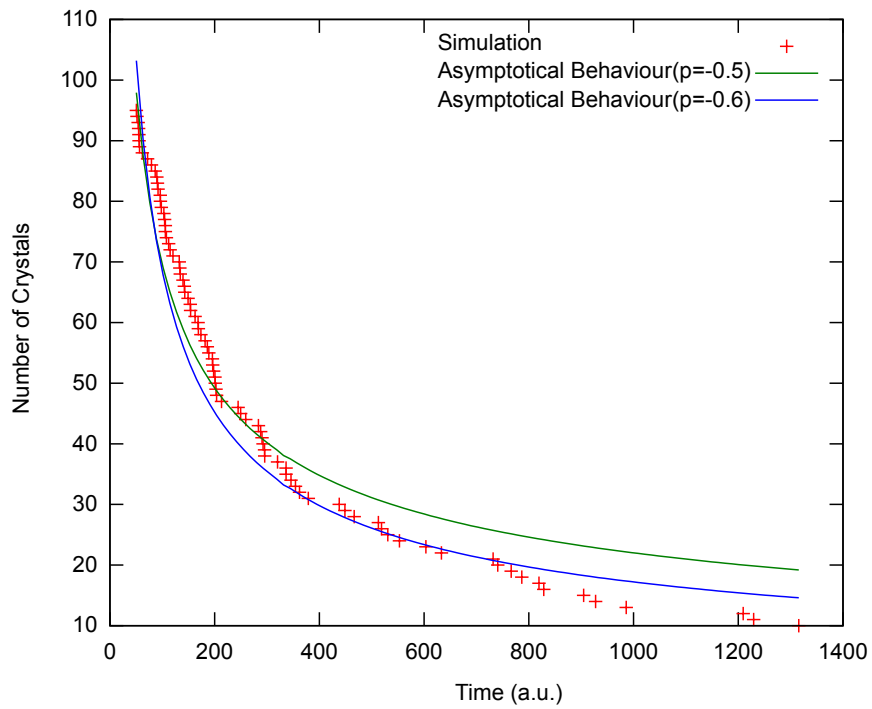


Figure 5.10: Number of Crystals over Time ($\theta = 0.3\pi$)

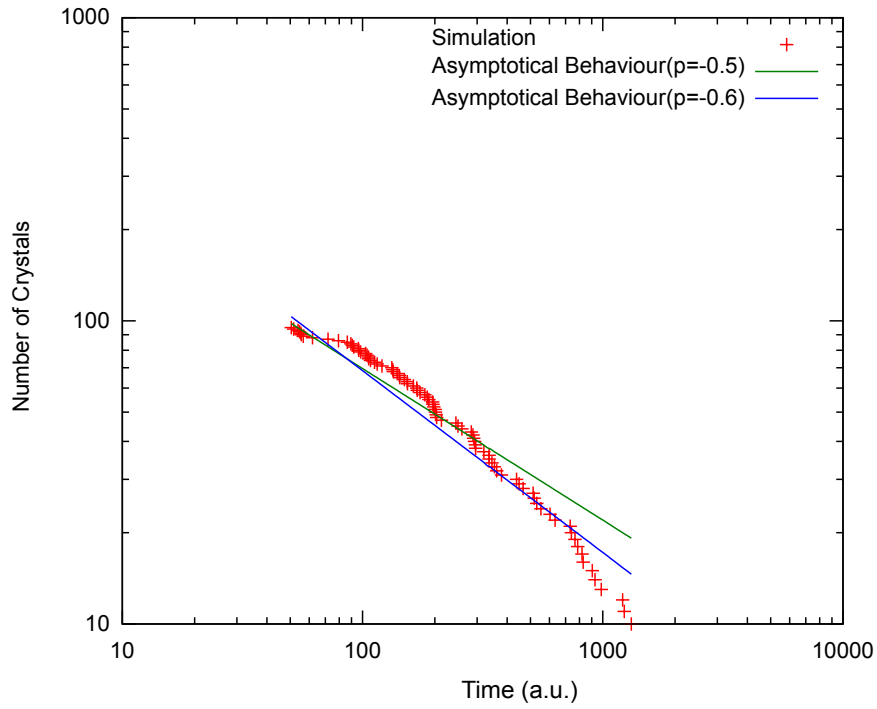


Figure 5.11: Number of Crystals over Time ($\theta = 0.3 \pi$, Logarithmic Scales)

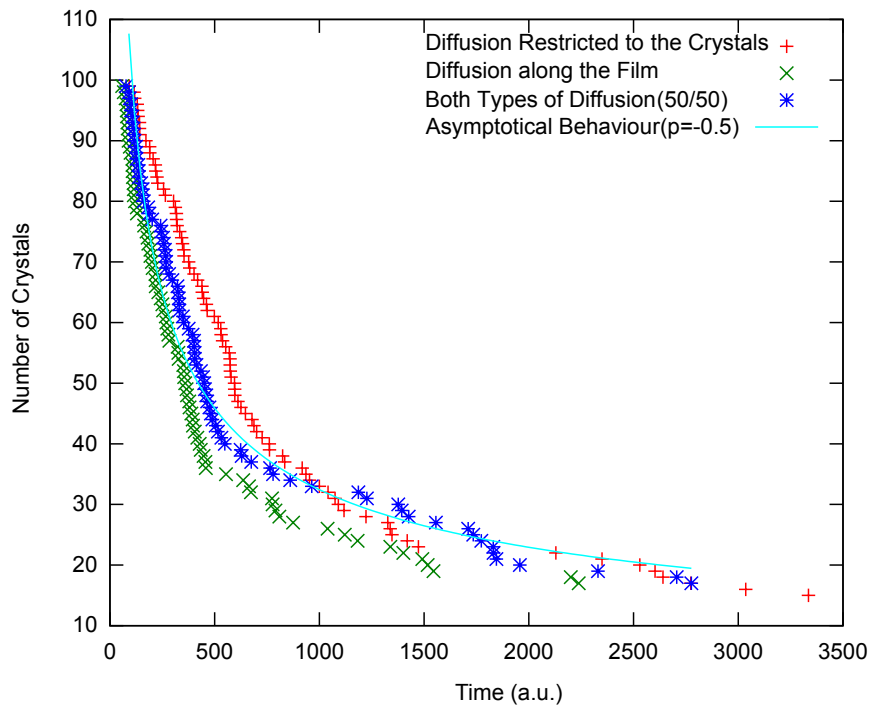


Figure 5.12: Number of Crystals over Time ($\theta = 0.5 \pi$)

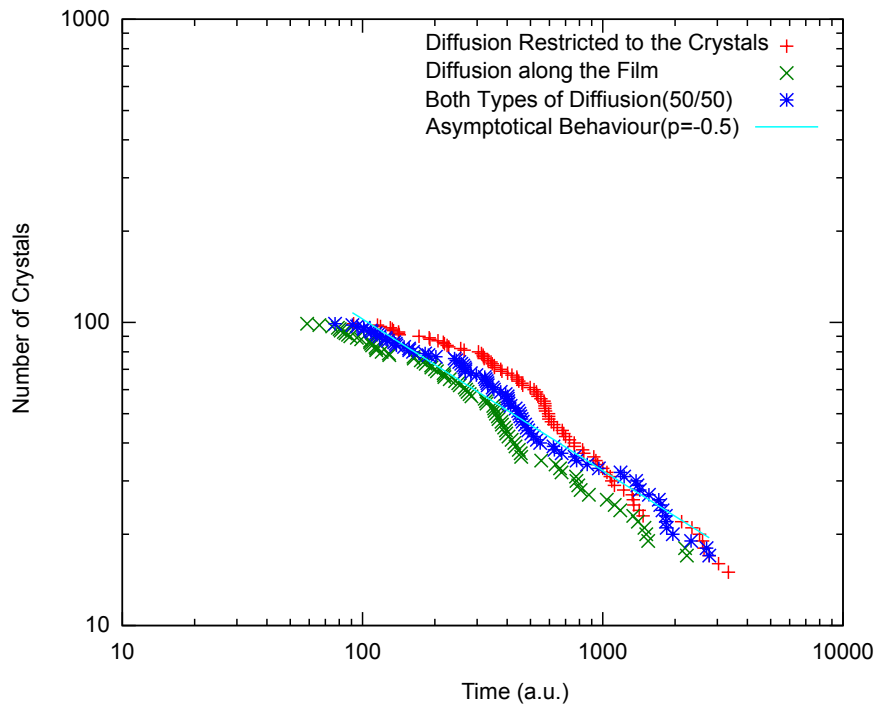


Figure 5.13: Number of Crystals over Time ($\theta = 0.5 \pi$, Logarithmic Scales)

The first case, which uses the law used throughout this section, again shows the familiar picture of the decrease of crystals not clearly following a power law. However, the equal mixture of the two choices for the normal growth rate exhibits interesting characteristics. Although deviating a little from the power law, the influence of the infinite diffusion along the whole film seems to be enough for it to hold.

With this transition an increasing sharpness of the distribution of the surviving angles is visible (see figure 5.14, 5.15 and 5.16).

The results of the simulations (figures 5.17 and 5.18) show the preference regarding the orientation, which is expected from these cases.

The result of another case of mixture of the two types of diffusion is shown in figures 5.19, 5.20 and 5.21, where the material comes from the right. We see that the diffusion along the substrate quickly dominates the behaviour of the evolution, even though we are using the same angle of incidence ($\theta = 0.3 \pi$) as before, which was chosen for the variety of growth speeds it creates. Figure 5.22 shows the decrease of the numbers of crystals and exhibits a familiar characteristic: Assuming only half the diffusion is limited to the crystal suffices for the asymptotic rate to be followed. With this comes a dominance of the angles near $\pi/4$, which is clearly visible in figure 5.23. As the results for $\theta = 0.7 \pi$, $\theta = 0.3 \pi$ and $\theta = 0.5 \pi$ are symmetrical, the corresponding figures are left out.

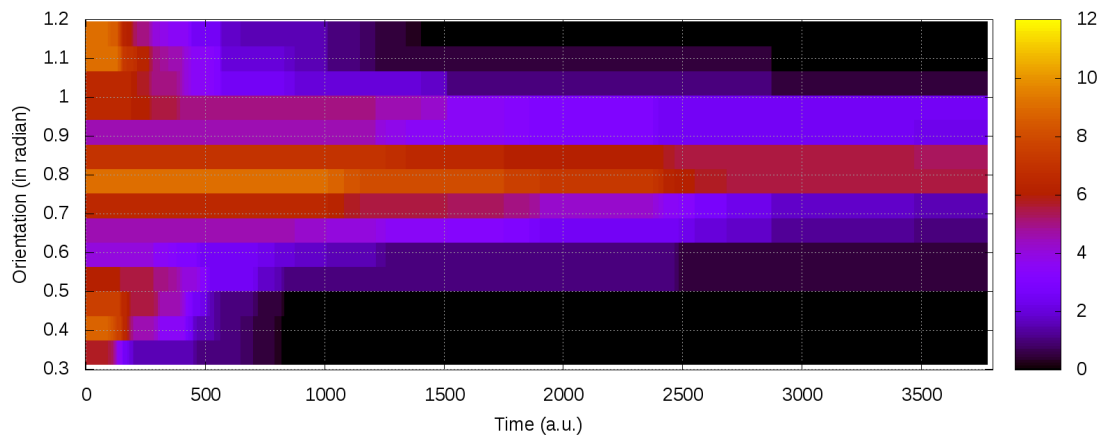


Figure 5.14: Material from the Middle, Material Diffusion Restricted to the Crystals

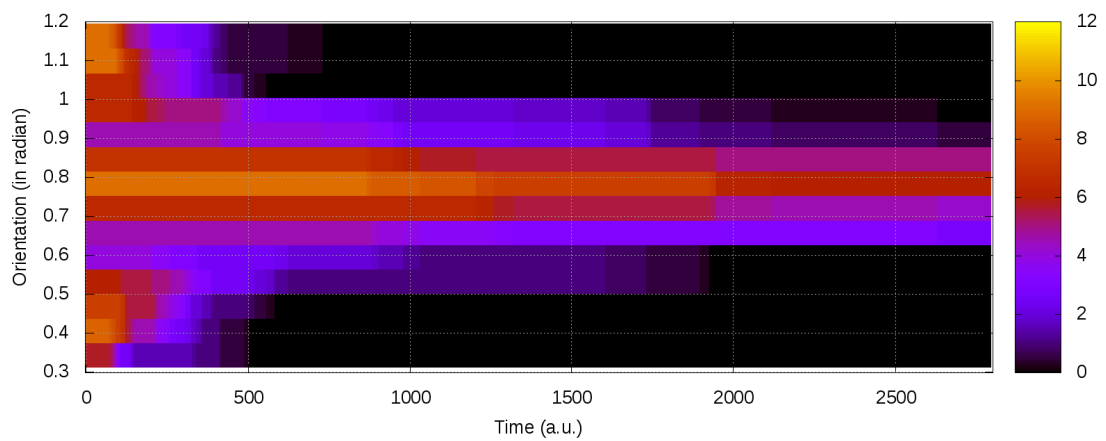


Figure 5.15: Material from the Middle, 75% Material Diffusion Restricted to the Crystals

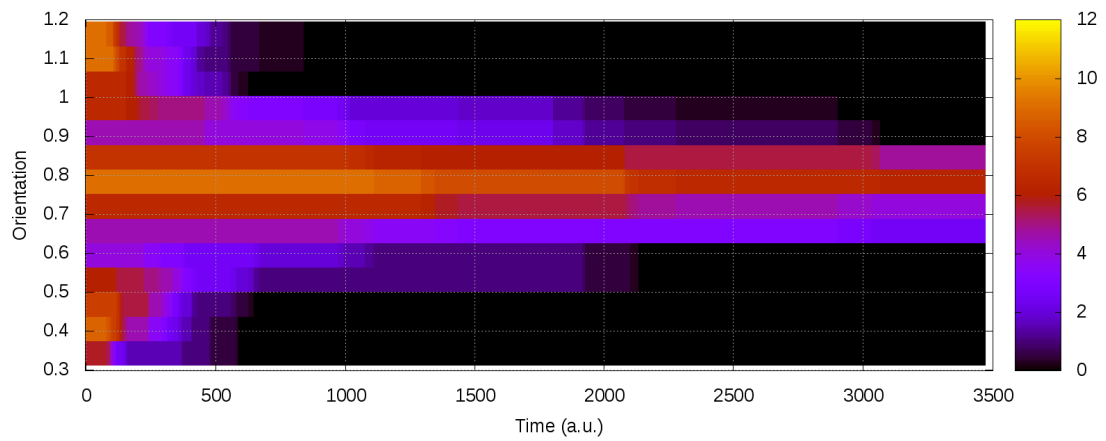


Figure 5.16: Material from the Middle, 50% Material Diffusion Restricted to the Crystals

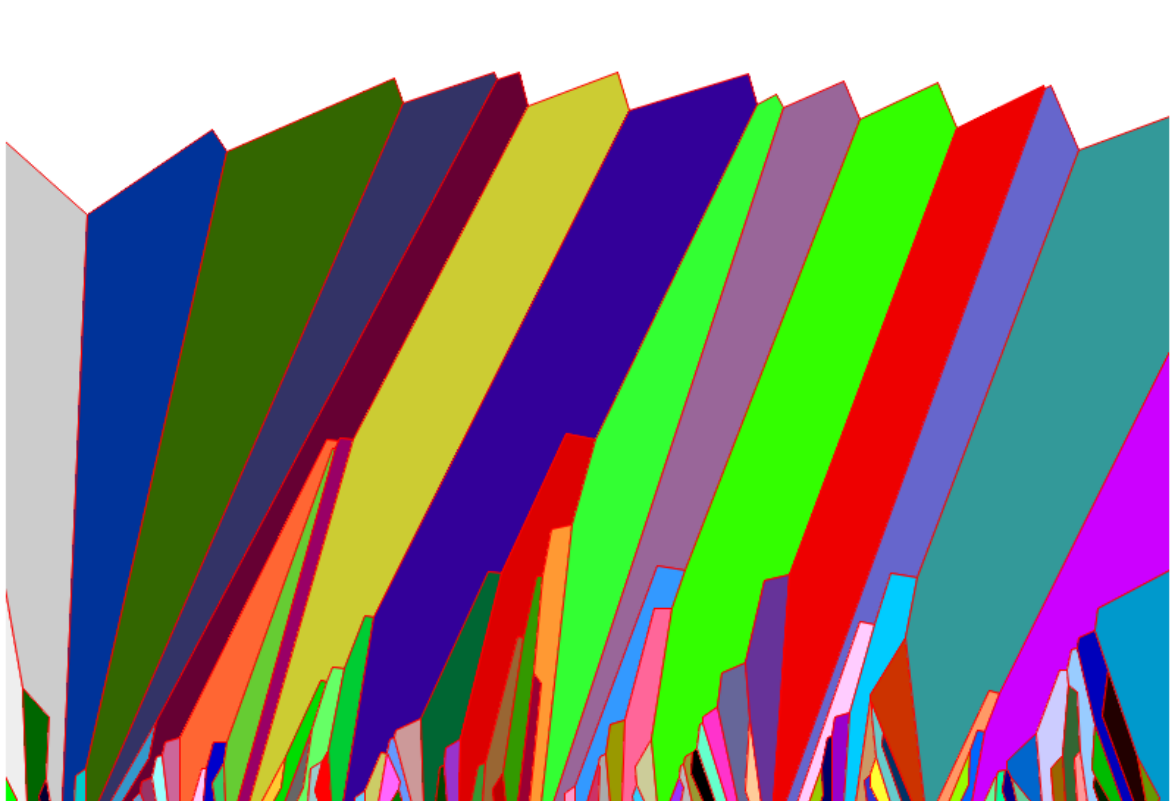


Figure 5.17: Material from the Left



Figure 5.18: Material from the Right

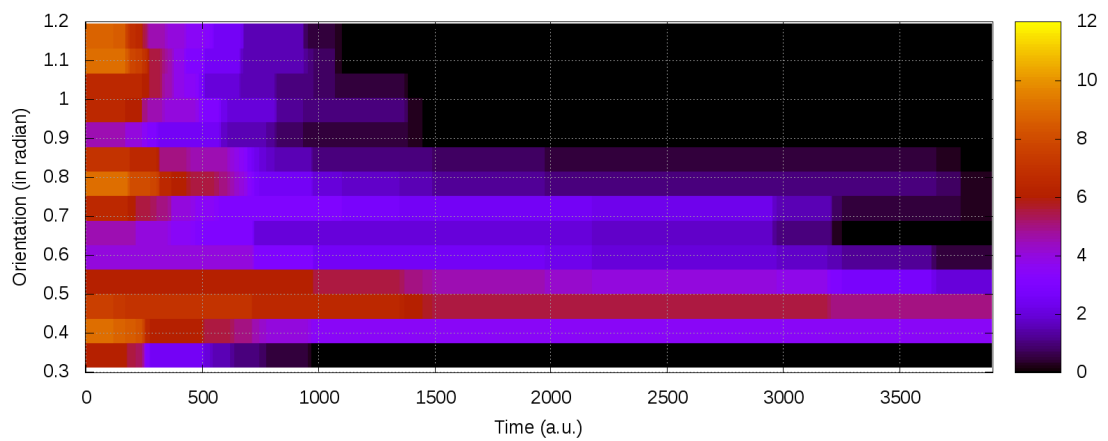


Figure 5.19: Material from the Right, Material Diffusion Restricted to the Crystals

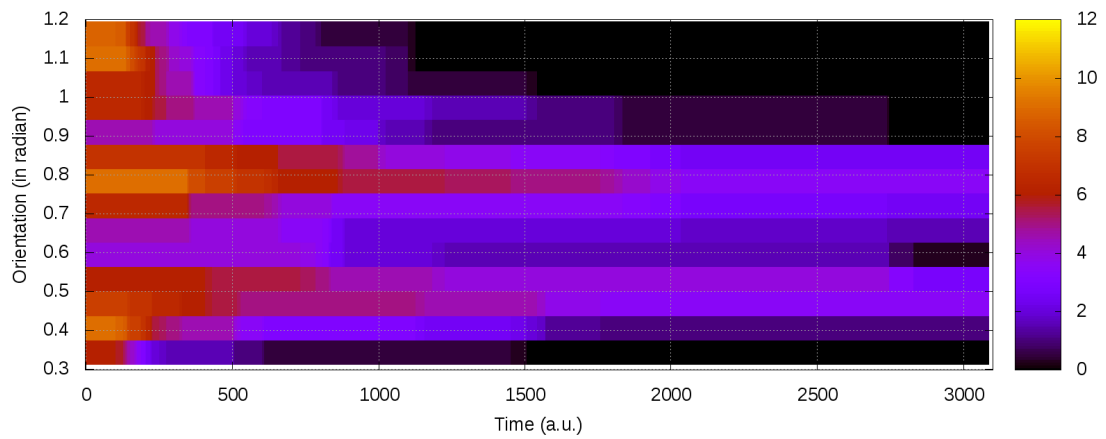


Figure 5.20: Material from the Right, 75% Material Diffusion Restricted to the Crystals

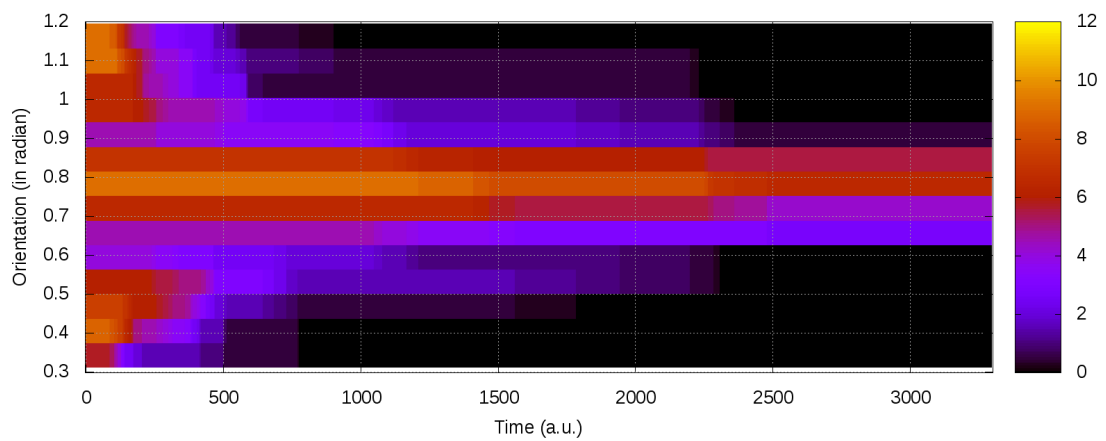


Figure 5.21: Material from the Right, 50% Material Diffusion Restricted to the Crystals

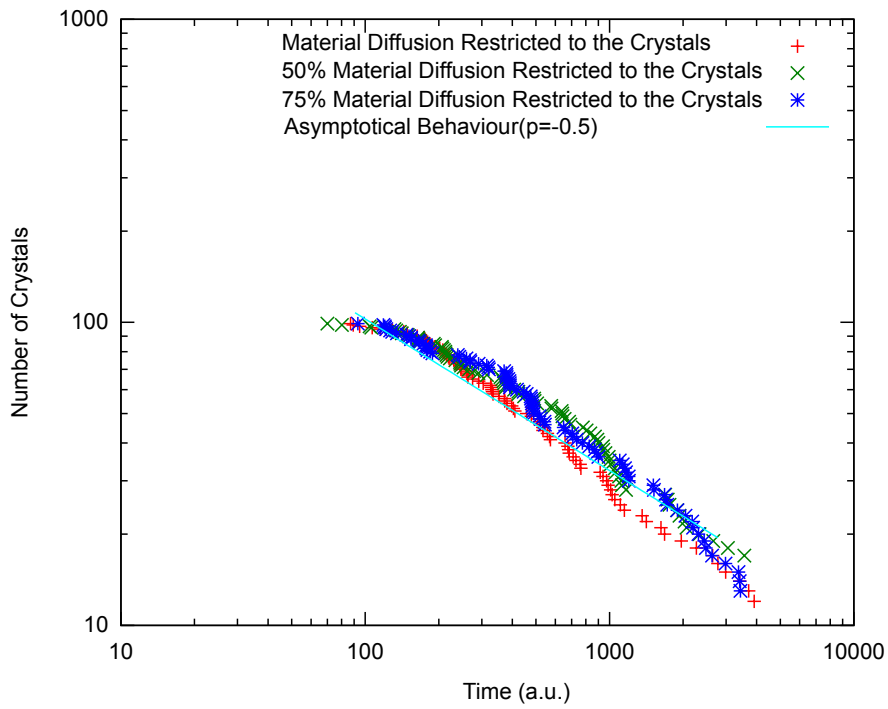


Figure 5.22: Number of Crystals over Time, Material Coming from The Right

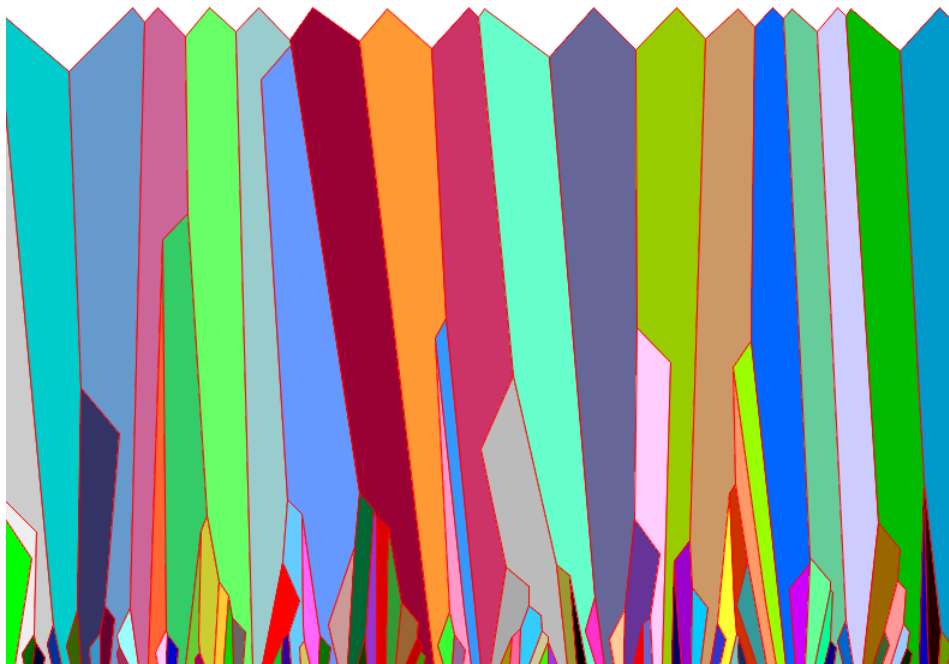


Figure 5.23: Simulation Result for Material from the right and 50% Material Diffusion restricted to the Crystals

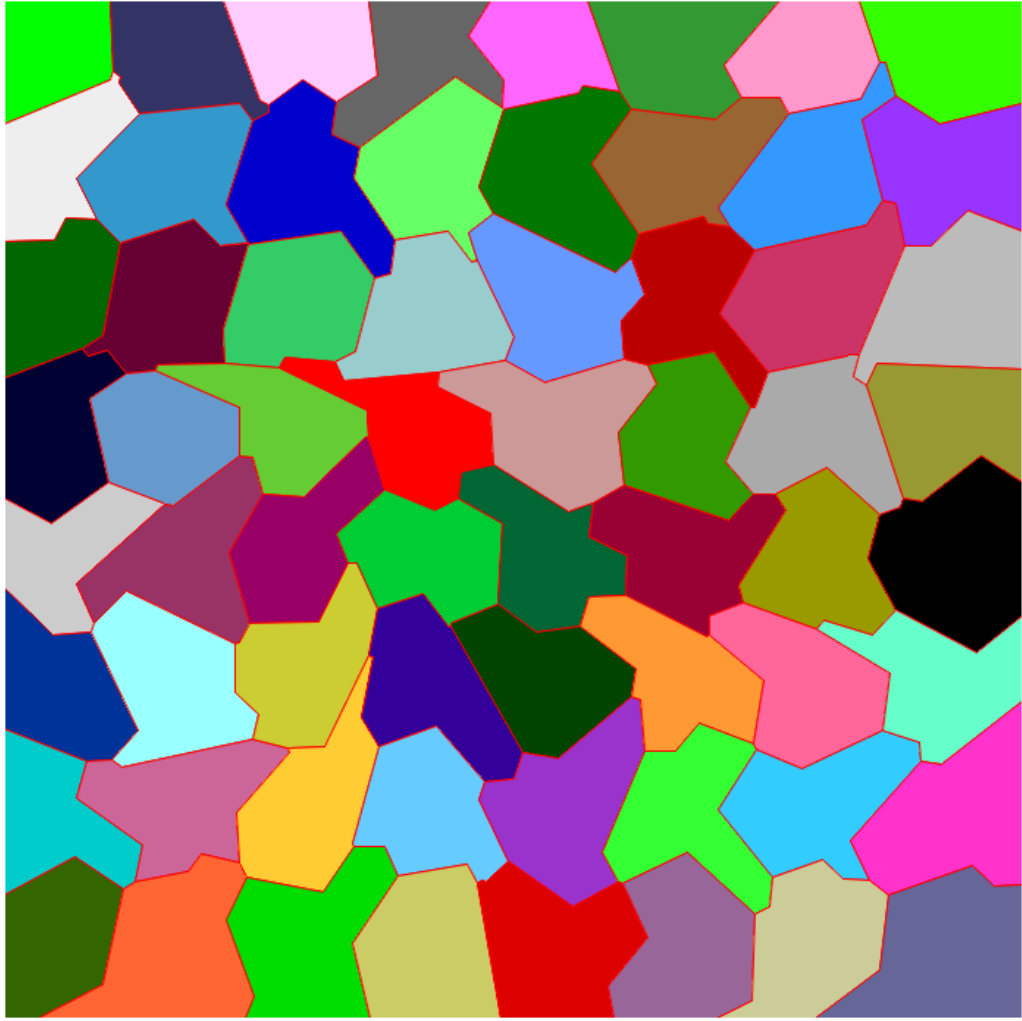


Figure 5.25: A General Two-dimensional Case

Chapter 6

Conclusion and Outlook

The proof for the average in-plane crystal size and its caveats were investigated, and compared them with the results of the simulations. The flexibility of the algorithm was shown by two examples. In addition to the classic example, another setting by restricting the diffusion to the separate crystals and the influence of the diffusion along the surface when mixed with it were looked at. The simulation of the classic case has been verified by a comparison with the theoretical result of asymptotical behaviour of the average in-plane crystal size. The problems in the proof [15] were highlighted and a possible solution was suggested.

The program allows to export the results of the simulation for postprocessing in mesh generators. On the resulting mesh it is possible to set the parameters of the grains and their boundaries and use it as an input for stress simulations calculating the distribution of the stress and its change with regard to e.g. temperature or force.

There are numerous possibilities of extending the algorithm introduced in this work. The most interesting extension is a three dimensional setting, which is certainly possible in a limited way using the two dimensional simulation program to calculate cross sections. The problem of combining these in a way to get a good representation of the three dimensional case remains, but it should be solvable for simple situations.

Bibliography

- [1] A. Van der Drift. Evolutionary Selection, a Principle Governing Growth Orientation in Vapour-Deposited Layers. *Phillips Res. Repts*, 22:267–288, 1967.
- [2] B. W. Sheldon, A. Ditekowski, R. Beresford, E. Chason, and J. Rankin. Intrinsic Compressive Stress in Polycrystalline Films with Negligible Grain Boundary Diffusion. *J. Appl. Phys.*, 94(2):948–957, 2003.
- [3] C. Tang, S. Alexander, and R. Bruinsma. Scaling Theory for the Growth of Amorphous Films. *Physical Review Letters*, 64(7):772–775, 1990.
- [4] C. V. Thompson. Structure Evolution During Processing of Polycrystalline Films. *Annu. Rev. Mater. Sci.*, 30:159–190, 2000.
- [5] C. Wild, N. Herres, and P. Koidl. Texture Formation in Polycrystalline Diamond Films. *Appl. Phys.*, 68:973, 1990.
- [6] G. Russo and P. Smereka. A Level-Set Method for the Evolution of Faceted Crystals. *SIAM J. Sci. Comput.*, 21(6):2073–2095, 2000.
- [7] G. Wiederhirn. *The Strengths Limits of Ultra-Thin Copper Films*. PhD thesis, Universität Stuttgart, 2007.
- [8] H. Ceric, A. Nentchev, E. Langer, and S. Selberherr. Intrinsic Stress Build-Up During Volmer-Weber Crystal Growth. In *Proc. Simulation of Semiconductor Processes and Devices*, pages 37–40, 2007.
- [9] H. Ceric, C. Hollauer, and S. Selberherr. Simulation of Texture Development Caused Stress Build-Up in Electroplated Copper Lines. In *13th International Symposium on the Physical and Failure Analysis of Integrated Circuits*, 2006.
- [10] H. Ceric, C. Hollauer, and S. Selberherr. Three-Dimensional Simulation of Intrinsic Stress Build-Up in Thin Films. *SISPAD*, pages 192–195, 2007.
- [11] I. M. Lifshitz and V. V. Slyozov. The kinetics of precipitation from supersaturated solid solutions. *Journal of Physics and Chemistry of Solids*, 19(1-2):35–60, 1961.
- [12] J. Cho, S. G. Terry, R. LeSar, and C. G. Levi. A Kinetic Monte Carlo Simulation of Film Growth by Physical Vapor Deposition on Rotating Substrates. *Materials Science and Engineering*, 391:390–401, 2004.

-
- [13] J. Debierre, A. Karma, F. Celestini, and R. Guérin. Phase-field Approach for Faceted Solidification. *Phys. Rev. E*, 68(4):041604, Oct 2003.
- [14] J. E. Taylor and J. W. Cahn. Diffuse Interfaces with Sharp Corners and Facets: Phase Field Models with Strongly Anisotropic Surfaces. *Physica D: Nonlinear Phenomena*, 112(3-4):381–411, 1998.
- [15] J. M. Thijsen, H. J. F. Knops, and A. J. Dammers. Dynamic Scaling in Polycrystalline Growth. *Phys. Rev.*, B45:8650, 1992.
- [16] M. F. Dorner and W. D. Nix. Stresses and Deformation Processes and Devices. *Solid State Mater. Sci.*, 14(3):225–267, 1988.
- [17] M. Opper and D. Saad. *Advanced Mean Field Methods Theory and Practice*. MIT Press, 2001.
- [18] N. Moelans, B. Blanpain, and P. Wollants. An Introduction to Phase-Field Modeling of Microstructure Evolution. *Calphad*, 32(2):268–294, 2008.
- [19] O. P. Karpenko, J. C. Bilello, and S. M. Yalisove. Growth Anisotropy and Self-Shadowing: A Model for the Development of In-Plane Texture during Polycrystalline Thin-Film Growth. *J. Appl. Phys.*, 82(3):1397–1403, 1997.
- [20] P. Smereka, X. Li, G. Russo, and D.J. Srolovitz. Simulation of Faceted Film Growth in Three Dimensions: Microstructure, Morphology and Texture. *Acta Materialia*, 53:1191–1204, 2005.
- [21] Paritosh, D. J. Srolovitz, C. C. Battaile, X.Li, and J. E. Butler. Simulation of Faceted Film Growth in Two-Dimensions: Microstructure, Morphology and Texture. *Acta Mater.*, 47:2269, 1999.
- [22] R. A. Roy and R. Messier. Evolutionary Growth Development in SiC Sputtered Films. *Mat. Res. Soc. Symp. Proc.*, 38:363, 1985.
- [23] S. Ruan and C. A. Schuh. Kinetic Monte Carlo Simulations of Nanocrystalline Film Deposition. *J. Appl. Phys.*, 107, 2010.
- [24] S. Wise, J. Kim, and J. Lowengrub. Solving the Regularized, Strongly Anisotropic Cahn-Hilliard Equation by an Adaptive Nonlinear Multigrid Method. *Journal of Computational Physics*, 226(1):414–446, 2007.
- [25] Jonathan Richard Shewchuk. Robust adaptive floating-point geometric predicates. In *in Proc. 12th Annu. ACM Sympos. Comput. Geom*, pages 141–150, 1996.
- [26] Sixth International Symposium on Silicon Materials Science and Technology. *2d - Computer Modelling of the Growth of Polycrystalline Films*, 1990.
- [27] W. D. Nix and B. M. Clemens. Crystallite Coalescence- A Mechanism for Intrinsic Tensile Stresses in Thin Films. *Journal of Materials Research*, 14(8):3467–3473, 1999.